MEMBER

REPORT

[*China*]

ESCAP/WMO Typhoon Committee
19th Integrated Workshop
AP-TCRC, Shanghai, China
19 – 22 November 2024

CONTENTS

I. Review of Tropical Cyclones Affecting China since Last Session of ESCAP/WMO Typhoon Committee

1.1 Meteorological and Hydrological Assessment

A moderate eastern type El Niño event has occurred since May 2023, lasting until May 2024. Since 2024, the Sea Surface Temperature (SST) in the tropical Pacific has shown the characteristics of reduced warming and a slowly transition towards to the La Niña phase. The Nino3.4 index has consistently turned to be negative since September, while the SST in the tropical Indian Ocean has remained warmer than usual. Under the influence of the decaying El Niño event and the warmer SST in the Indian Ocean, the northwestern Pacific subtropical high (SH) has remained persistently stronger with the affected areas being larger. The ridge of SH is close to the long-term average, with the western extension point shifted further west. Thus, the SH affects the area where tropical cyclones (TCs) genesis, and suppresses TCs activity in spring and summer. It wasn't until September that the SH shifted northward compared to the long-term average, resulting in increased TCs genesis.

From 1st January to 4th November 2024, the Western North Pacific (WNP) and the South China Sea (SCS) have witnessed the formations of 22 TCs, which is 0.37 less than the average number of multiple years during the same period (22.37). Among of these named TCs, 8 of them made landfall in China, which is slightly higher than the average number

(7.1) for the climatological period. Tropical Storm Maliksi (2402) made landfall in Yangjiang, Guangdong Province on 1st June, 2024. Super Typhoon Gaemi (2403) made landfall in Yilan, Taiwan Province and Putian, Fujian Province on 25th July successively. Severe Tropical Storm Prapiroon (2404) made landfall in Wanning, Hainan Province on 22th July. Super Typhoon Yagi (2411) made landfall in Wenchang, Hainan Province and Xuwen, Guangdong Province on 6th September successively. Severe Typhoon Bebinca (2413) made landfall in Pudong District of Shanghai on 16th September. Severe Tropical Storm Pulasan (2414) made landfall in Zhoushan, Zhejiang Province and Fengxian District of Shanghai on 19th September successively. Super Typhoon Krathon (2418) made landfall in Kaohsiung, Taiwan Province on 3rd October. Super Typhoon Kong-Rey (2422) made landfall in Taitung, Taiwan Province on 31th October.

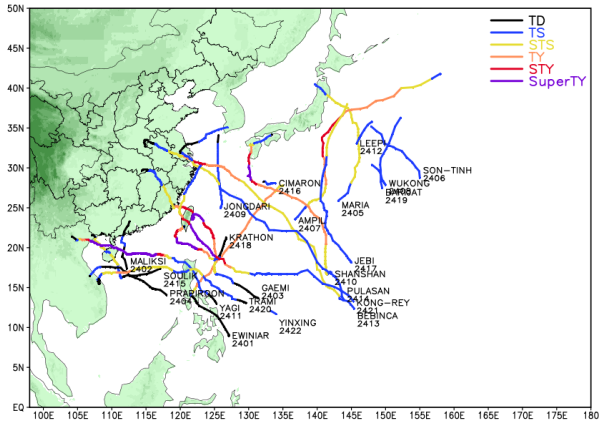

Fig. 1.1 Tracks of TCs over the WNP and the South China Sea from 1st January to 4th November 2024.

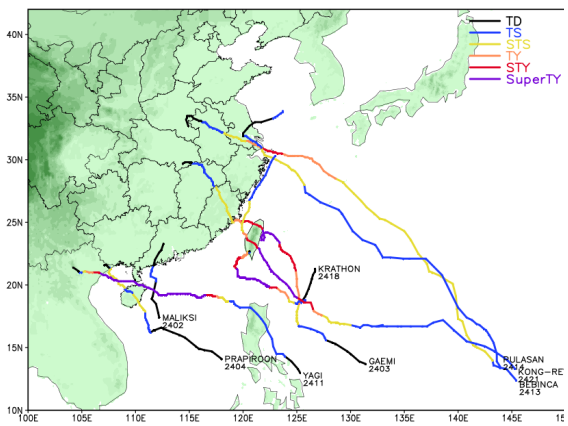

Fig1.2 Tracks of 7 TCs that made landfall over China from 1st January to 4th November 2024.

1.1.1 Characteristics of TCs in 2024

In 2024, TCs activity has exhibited the several following characteristics. The genesis area shifted further west and north with a lower number of genesis. The number of TCs landfalls is equal to the climatological average but with stronger intensity. The period of TCs genesis is concentrated with more TCs are active during the Autumn.

1) Westward and Northward TCs Genesis

By 4th November, the average genesis location for the 22 TCs this year is 19.82°N, 134.27°E. This shows a northward deviation of nearly 3.7 degrees in latitude and a westward deviation about 2.5 degrees in longitude compared to the climatology of 16.16°N, 136.76°E (Fig. 1.3).

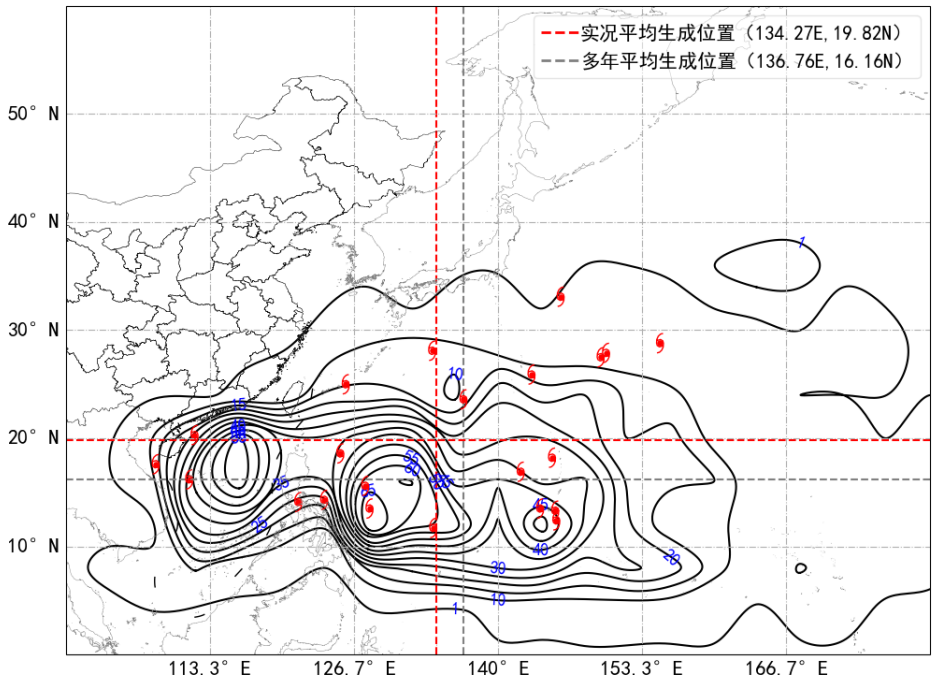

Fig. 1.3 WNP and SCS tropical cyclone source region density distribution (black lines and dashed line for latitude & longitude averaged, resolution: 2.5°×2.5°, climatology from 1949 to 2021) and genesis location of tropical cyclones (red typhoon symbols and dashed lines for latitude & longitude averaged) forming from 1st January to 4th November 2024.

2 TCs Genesis with Lower Average Intensity

As of 4th November, 22 TCs generated in the WNP and the SCS, which is less than the climate average. With the exception of surpluses in May, August and September, the number of TCs in other months is below the average. Specifically, in September, there were 3.0 TCs more than climatology mean value, meanwhile 1.8 fewer in July. The average maximum intensity for TCs this year is 34.1m/s, which is 3.2m/s weaker than the climatological mean value 37.3m/s as shown in Fig. 1.4.

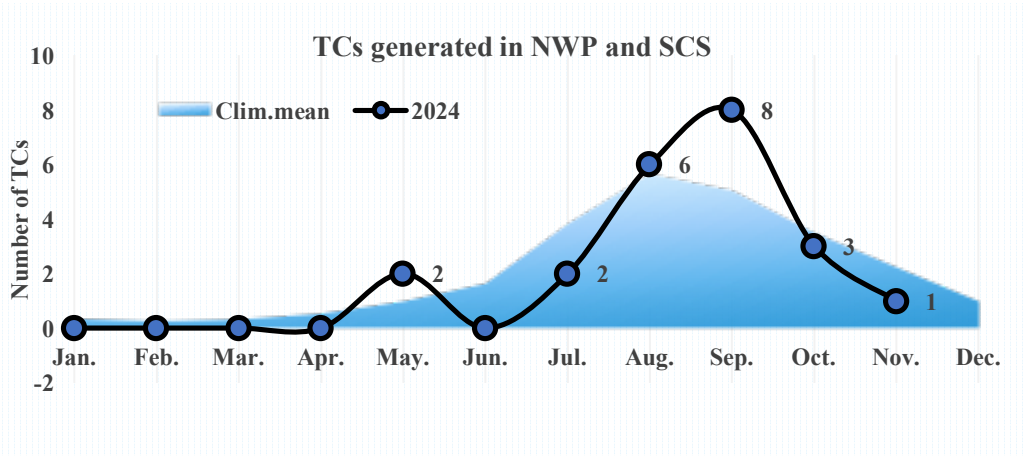

Fig. 1.4 Monthly distribution of TCs generated in WNP and the South China Sea in 2024 (blue line) and that for climatological mean (1991-2020, blue shadings).

3 More Landfall TCs with higher intensity

In 2024, there are 8 TCs making landfall in China, which is slightly higher than the climatology mean value in the same period in previous years. The landing positions include Guangdong, Zhejiang, Taiwan, Hainan provinces and Shanghai. The average landfall intensity of these 8 TCs is 38.6m/s (for those make landfall more than one time, only the first

landfall was taken into account), remarkably stronger by 6.1m/s compared to the annual average being 32.5m/s.

Among the 8 landfall TCs, Super Typhoon Yagi (2411) made landfall in Wenchang, Hainan Province on 6th September with the maximum sustainable wind up to 62m/s (over 17 Beaufort scale,), which is the strongest TC made landfall in China during autumn. Severe Typhoon Bebinca (2413) made landfall in Pudong District of Shanghai on 16th September with maximum sustainable wind of 42m/s (14 Beaufort scale), which is the strongest landfalling TC in Shanghai since 1949. Super Typhoon Krathon (2418) made landfall in Kaohsiung, Taiwan Province on 3rd October with maximum sustainable wind of 38m/s (13 Beaufort scale), which is the strongest typhoon made landfall in Kaohsiung since 1977.

4 Concentrated landfalling areas and time

The landfall areas are concentrated, with the landfalling of Severe Typhoon Bebinca (2413) and Severe Tropical Storm Pulasan (2414) in eastern China and within 4 days in September successively. The multiple occurrences of extreme rainfall events in eastern China due to these two landfall TCs. Super Typhoon Krathon (2418) and Kong-Rey (2421) both made landfall in eastern coastline of Taiwan in October successively, with the additive effects of precipitation related with these two TCs induced severe disaster to Taiwan.

5 More active TCs in the Autumn

Since the beginning of autumn this year (September 1st to November 4th), a total of 12 TCs have been generated in the NWP and SCS, 2.9 more than the climatological mean value (9.1). Among those Autumn TCs, 5 of them made landfall in China successively, which is comparably twice to the climatological mean. Due to common influence from cold air and landfall TCs, severe gust winds and rainfall occurred in southern and eastern China, with the daily rainfall in many places broke the historical extreme record.

1.1.2 Precipitation of TCs Affecting China

Affected by the rainfall associated with 8 landfall TCs, 468 rivers across 25 provinces in China have experienced floods exceeding warning levels. Among them, Super Typhoon Gaemi (2403) caused the most significant impact, which is mainly characterized by the following three aspects.

1) Wide-ranged Impact

Affected by Super Typhoon Gaemi (2403), from 25th July to 31th July, a large-scale strong rainfall process occurred in Southern and Eastern China, the eastern and southern parts of Southwest China, the southeastern part of Northwest China, the Huang-Huai region, North China, and Northeast China. The areas covered by cumulative rainfall amounts of 250

mm, 100 mm, and 50 mm were 94,000, 1.014 million, and 2.325 million square kilometers, respectively.

2) Severe Accumulated Rainfall

The maximum accumulated point rainfall during the process was 718 mm in Pingshi, Chenzhou, Hunan Province, 630 mm in Shuimen, Ningde, Fujian Province, and 532 mm in Longwang Temple, Fengcheng, Dandong, Liaoning Province.

3) Several Rivers Exceeding Warning Levels

In the Pearl River Basin, the Han River, Songhua River, and Yangtze River have experienced 4 numbered floods. Floods exceeding warning levels occurred in 282 rivers across 21 provinces, 78 rivers experienced floods exceeding the guarantee level, and 8 rivers experienced floods exceeding historical records (Fig. 1.5).

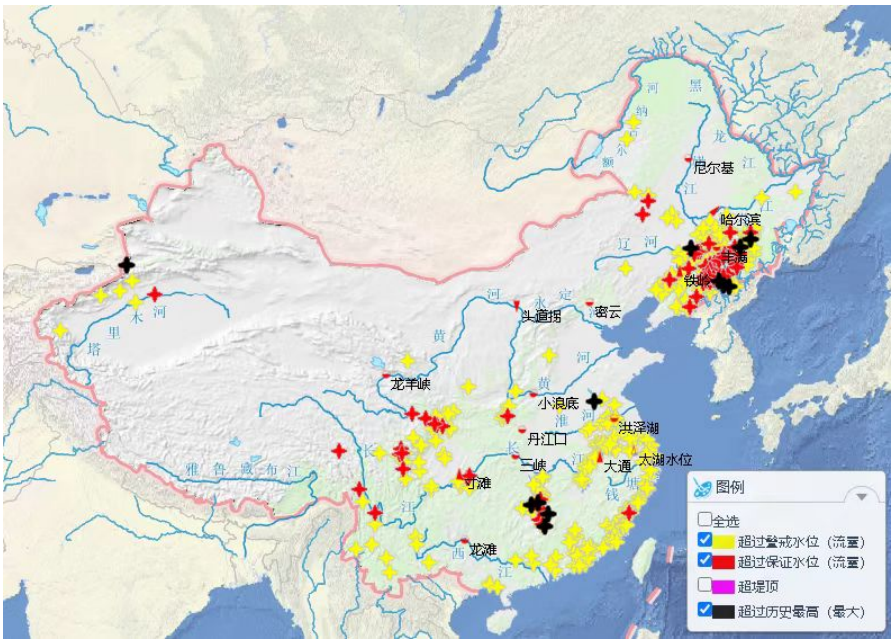

Fig. 1.5 Rivers exceeding the warning level under the effects of Super Typhoon Gaemi (2403)

1.1.3 TCs Affecting China

1) Tropical Storm MALIKSI (2402)

Tropical Storm Maliksi generated over the northwestern part of the South China Sea at 06:00UTC on 31th May, then it moved northward before landfall. On the 31th May 16:55UTC, Maliksi made landfall as a tropical storm along the coast of Yangjiang, Guangdong Province (maximum wind speed of 18m/s and minimum central pressure 998hPa). After landfalling, Maliksi weakened into a tropical depression and continued to move northeast over Guangdong Province. It finally dissipated in Guangdong Province.

Due to the impact of Maliksi, from 31th May to 1st June, the accumulated rainfall in Zhejiang, Fujian, Guangdong, most parts of Hainan and some areas of Guangxi reached 50~100mm, locally reaching over 100mm. The wind gust over most coastal areas of Guangdong reached Beaufort scale (Bft)-7 to 8.

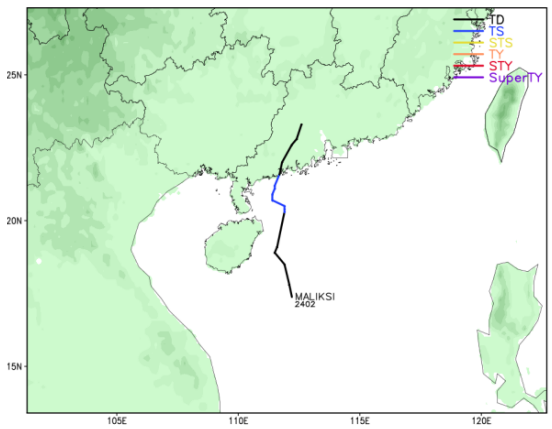

Fig. 1.6 (a) Track of Maliksi(2402)

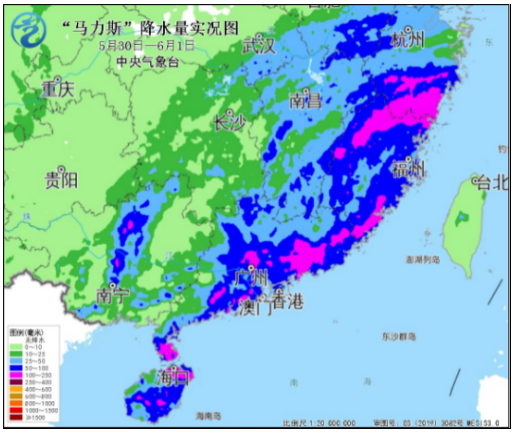

Fig. 1.6 (b) Accumulated rainfall of Maliksi(2402)

2) Super Typhoon GAEMI (2403)

Super Typhoon Gaemi generated over to the east of the Philippines at 06:00UTC on 20th July. It initially moved northward then shifted northward. By 06:00UTC on 21th July, it intensified into a severe tropical storm, then by 12:00UTC on 22th July, it further intensified into a typhoon. At 09:00UTC on 23th July, it reached the status of a severe typhoon and by 00:00UTC on the 24th July, it intensified as a super typhoon. It maintained super typhoon when counterclockwise spinning over the northeast offshore of Taiwan Island, then made landfall along the coastal areas of Yilan, Taiwan Province, as a severe typhoon (48m/s, 945hPa) around 16:00UTC on the 24th July. Then after crossing the northern part of Taiwan Island, Gaemi entered the Taiwan Strait with its intensity gradually weakened, and made its second landfall in the coastal area of Putian, Fujian Province as a typhoon(33m/s, 972hPa) around 11:50UTC on the 25th. After landfalling, the intensity of Gaemi weakened slowly, and moved northwestward. It entered Jiangxi Province from Fujian Province around 09:00UTC on the 26th. Then, it entered Hubei Province around 09:00UTC on the 27th, and weakened into a tropical depression.

Affected by Gaemi and its remnant system, from the 24th to the 28th July, the accumulative rainfall in Taiwan, Fujian, Eastern and Southern Zhejiang, Central and Southern Jiangxi, Eastern Hunan, Southeastern Hubei, Central and Northern and Eastern Guangdong, and Northeastern

Guangxi reached 100~300mm, and that in Ningde, Fuzhou, Putian, Quanzhou of Fujian Province, Wenzhou of Zhejiang Province, Chaozhou, Jieyang, and Shantou of Guangdong Province, Chenzhou, and Zhuzhou of Hunan Province attained 400 to 875mm, and that in Central and Southern Taiwan reached 1000 to 1922mm. In addition, during the night of 24th July, the accumulated rainfall in Central and Eastern Liaoning and Eastern Jilin has reached 100~300mm, Shenyang, Anshan of Liaoning Province, Tonghua of Jilin Province reached 400 to 557mm, with maximum of 650.1mm in Zhujiafang, Shenyang, Liaoning Province. The daily precipitation of 14 national meteorological observation stations in Liaoning, Hunan, Jiangxi has broken the extremely historical record. Due to the heavy rainfall caused by Gaemi, 4 flooding events occurred in China, including Hanjiang River of the Pearl River Basin, Songhua River and Yangtze River. The water level of 282 rivers in 21 provinces including Fujian, Guangdong, Hunan, Shaanxi, Liaoning, Jilin, Heilongjiang etc. exceeded the warning water level with a range of 0.01~5.30m, 78 rivers exceeded guaranteed water level, and 8 rivers claimed the historical flood water level.

Super Typhoon Gaemi affected approximately 338,000 people in Guangdong Province, 765,000 people in Fujian Province, 178,000 people in Zhejiang Province, 44,000 people in Jiangxi Province, and 80,000

people in Hunan Province, resulting in the total directly economic loss was about 4.56 billion yuan, with 21.4 thousand hectares of crops affected.

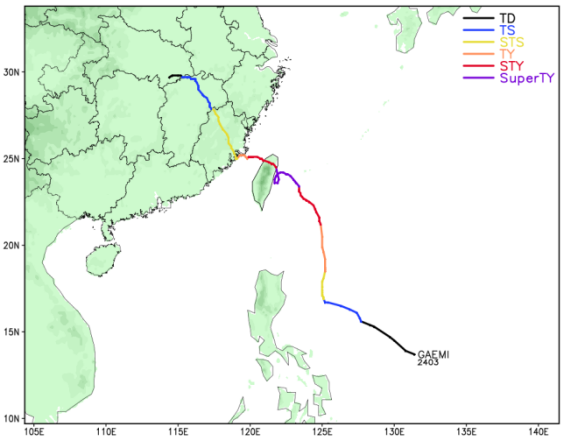

Fig. 1.7(a) Track of Gaemi (2403)

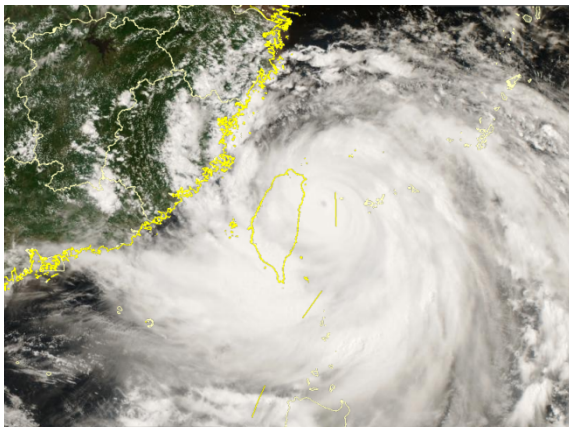

Fig. 1.7(b) FY-4B Satellite image at 06:30UTC 24th July.

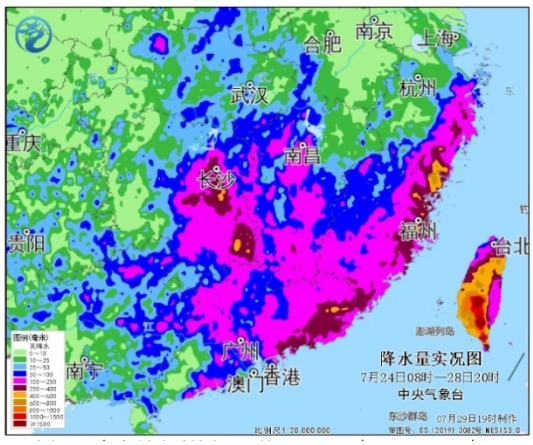

Fig. 1.7(c) Accumulated rainfall from 00:00UTC 24th to 12:00UTC 28th July.

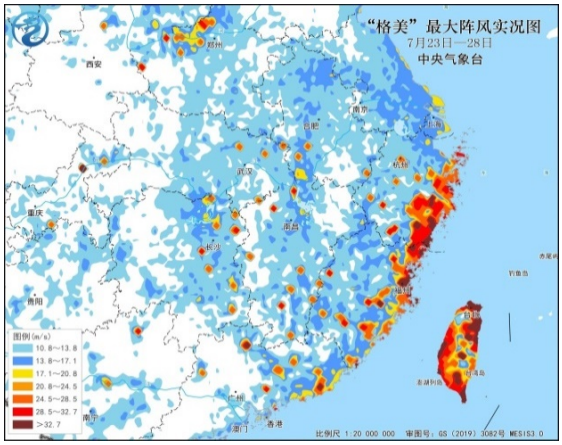

Fig. 1.7(d) Maximum wind gust from 23th to 28th July.

Fuzhou and Quanzhou of Fujian Province suspended work (business), production, classes, and closed markets on the 25th July, 70 passenger traffic routes in Zhoushan suspended on the 24th July, and 49 passenger transport routes suspended in Wenzhou of Zhejiang Province. Affected by heavy rain and flooding, supplies of water, electricity and network were cut off in 3 towns in Chenzhou, Hunan Province. Landslide causing casualties occurred in Shouyue, Nanyan, Hengyang, Hunan Province on

the 28th July. A breach occurred at the Sixin Dyke in Xintang, Yishu River, Xiangtan, Hunan Province.

3) Severe Tropical Storm PRAPIROON (2404)

Severe Tropical Storm Prapiroon generated over the central part of the South China Sea at 21:00UTC on 20th July, then it moved northwestwards and gradually intensified. After landfalling in the coastal area of Wanning, Hainan Province as a severe tropical storm (28m/s, 985hPa) around 17:30UTC on the 21th, it gradually weakened into a tropical storm. Prapiroon (2404) moved across Hainan Island and entered Beibu Gulf at 01:00UTC 22th, then strengthened again to a severe tropical storm. Around 22:10 UTC 22th, it rapidly weakened into a tropical depression in Vietnam.

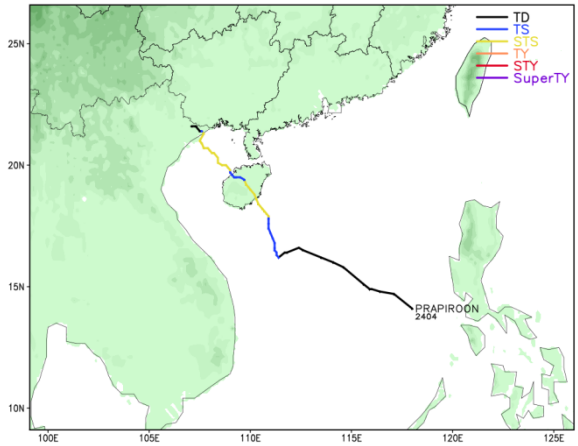

Fig. 1.8 (a) Track of Prapiroon (2404)

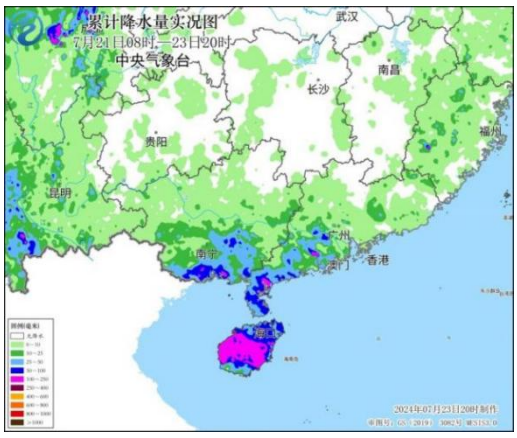

Fig. 1.8 (b) Accumulated rainfall from 00:00UTC 24th to 12:00UTC 23th July

Influenced by Prapiroon (2404) and its remnant system, from 21th to 23th July, the cumulative rainfall in Hainan Island, the southern coast of Guangxi Province, and the central and western coast of Guangdong

Province reached 50 ~100mm, among which the rainfall over central and northwestern parts of Hainan Island attained 150~245mm. The maximum hourly rainfall in the some above mentioned areas reached 40 to 74mm. The Bft 7-9 wind gusts were observed in the central eastern and coastal areas of Hainan Island, the southern coast of Guangxi Province, and the southwestern and coastal areas of Guangdong Province, with local gusts being Bft 10 to 13.

4) Super Typhoon YAGI (2411)

Super Typhoon Yagi generated over the east of the Philippines at 15:00UTC 1st September. It then moved northwestward and made landfall at 06:30UTC 2nd September as a tropical storm (20m/s, 995hPa) on the eastern coast of Luzon Island in the Philippines. Subsequently it crossed Luzon Island and entered into northeastern of the South China Sea, rapidly intensified from to Super typhoon. Then it moved westward with enhanced intensity. Around 08:20UTC 6th, it made its second landfall as a Super typhoon (62m/s, 915hPa) on the coast of Wenchang, Hainan Province. After landfalling, Yagi (2411) crossed the northern part of Hainan Island and entered into Qiongzhou Strait around 12:30UTC during the night, with its third landfall at 14:20UTC on the coast of Jiaowei, Xuwen, Guangdong Province as a Super typhoon (58m/s, 925hPa). Subsequently, it continued to move westward then shifted to northwest and entered Beibu Gulf, and

its intensity strengthened again. Around 08:20UTC 7th September, it made its fourth landfall on the coast of Quang Ninh Province, Vietnam. After this final landfalling, it rapidly weakened into a tropical depression in Vietnam around 03:00 UTC 8th. Yagi (2411) is the strongest typhoon that make landfall in China during autumn since meteorological records began, also the strongest typhoon in the Beibu Gulf.

Super Typhoon Yagi (2411) caused extensive impact due to the related gale wind and heavy rainfall, especially the severe wind gusts. Large scale gusts and rainfall have occurred on Hainan Island, southern Guangdong Province and southern Guangxi Province. The area of wind above 8 Bft in southern and coastal areas of South China is 78,600 square kilometers, and the area of wind above 10 Bft is 43,700 square kilometers. The observed wind of some buoy stations in the northern part of Hainan Island, Leizhou Peninsula, the northern part of the South China Sea, and the northern part of the Beibu Gulf was up to 15~17 Bft. In South China, the accumulative rainfall over 100mm covers 90,800 square kilometers and that over 250mm covers 13,200 square kilometers. Among them, the accumulative precipitation of some areas in the northern and western parts of Hainan Island, Shenzhen and Maoming in Guangdong Province, Fangchenggang and Qinzhou in Guangxi Province reached 300 to 500mm, and locally in Ledong, Hainan Province, the accumulative rainfall attained 691.2mm.

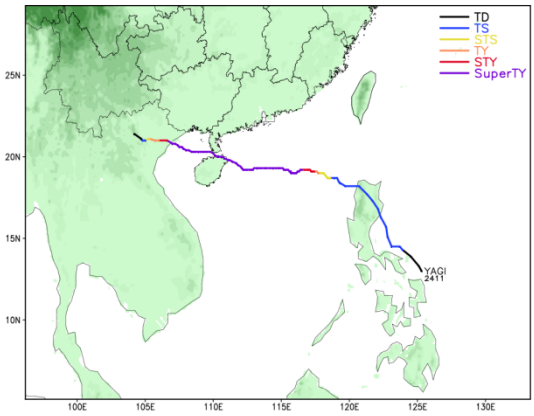

Fig. 1.9 (a) Track of Yagi (2411)

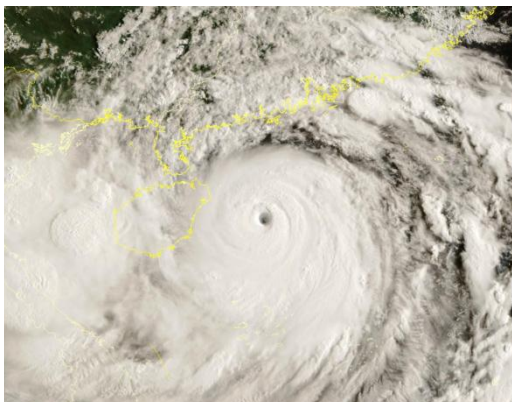

Fig. 1.9 (b) FY-4B Satellite image at 00:00UTC 6th September.

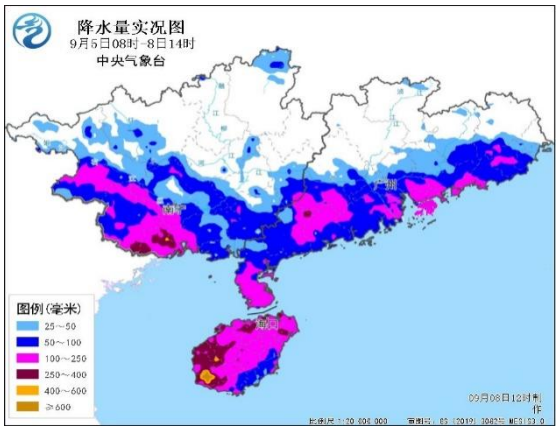

Fig. 1.9 (c) Accumulated rainfall from 00:00UTC 5th to 06:00UTC 8th September.

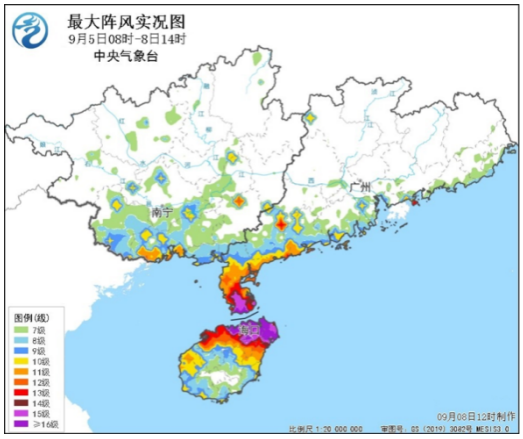

Fig. 1.9 (d) Maximum wind gust from 00:00UTC 5th to 06:00UTC 8th September.

Fig. 1.9 (e) Disasters caused by Yagi (2411) in Hainan

Fig. 1.9 (f) Wind turbine tower losses in Hainan

Yagi (2411) severely impacted urban operations, infrastructure, transportation, agricultural production, and the ecological environment in landfalling regions. According to the reports of local meteorological departments, there were widespread outage of electricity, disruptions of

water and gas supplies, fallen trees, cut off roads and damaged buildings in the areas near the landfalling location.

5) Super Typhoon BEBINCA (2413)

Typhoon Bebinca (2413) generated on the Northwest Pacific Ocean on 10th September at 12:00UTC. It initially moved in a northwesterly direction, gradually increasing in intensity. By 14th September at 15:00UTC, it intensified into a typhoon and entered the northern of the East China Sea. Around 15th September 23:00UTC, it made landfall on the coastal areas of Lingang New City, Pudong, Shanghai, as a severe typhoon (42m/s, 955hPa), which was the strongest typhoon to hit Shanghai since 1949. After making landfall, Bebinca (2413) continually moved in a west-northwesterly direction and slowly weakened. It entered Jiangsu Province around 16th September 03:00UTC. It was the strongest typhoon to enter Jiangsu since 1949. Then, it further weakened into a tropical depression around 17th September 08:00UTC and moved into Henan Province around 18:00UTC on the same day. Its remnant circulation remained over Henan for an extended period, causing severe wind and rainfall.

From 16th to 17th September, in Shanghai, central and southern Jiangsu, eastern Anhui and other places, there were wind gusts reaching Bft-8 to 10, with parts of Shanghai and the southern Jiangsu having Bft-12 to 14. A total of 35 national meteorological observation stations in

Shanghai, Jiangsu, Anhui and other places saw maximum gusts breaking the September records, with 10 stations in Shanghai and Jiangsu breaking the historical records.

From 15th to 19th September, accumulated rainfall in some areas in northern Zhejiang, Shanghai, southern and western Jiangsu, eastern Anhui, eastern Henan, southern Shandong, etc, received 50~150mm. The southern and northwestern Jiangsu, northeastern Anhui, eastern Henan, southwestern Shandong, and other areas received 200~300 mm of rainfall. Anhui Suzhou and Huaibei, Jiangsu Xuzhou, Henan Shangqiu, witnessed local accumulations of 350~550 mm, with rainfall over 630mm in Dangshan in Suzhou, Anhui, over 626 mm in Yucheng in Shangqiu, Henan. Eleven national observation stations in Anhui Suzhou and Huaibei, Jiangsu Xuzhou, Henan Shangqiu, Shandong Heze and other areas experienced record-breaking daily rainfall in September.

Bebinca (2413) has caused serious impacts in Shanghai, Jiangsu, Zhejiang, Anhui, Henan and Shandong province. According to the National Disaster Reduction Center of China, total 420,000 people in Shanghai, 312,000 people in Jiangsu and 395,000 people in Zhejiang were affected. Tragically, the direct economic losses amounted to 550 billion RMB, and approximately 15.9 thousand hectares of crops were affected. In addition, heavy rainfall and flooding caused by the remnants of Bebinca led to 243,000 people being affected in Suzhou, Anhui Province, with 38.2

thousand hectares of crops affected and a direct economic loss of 200 million RMB.

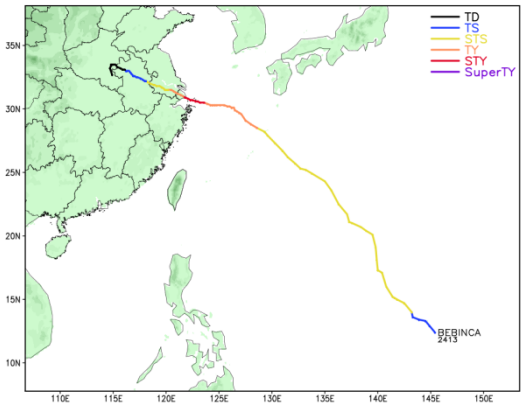

Fig. 1.10 (a) Track of Bebinca (2413)

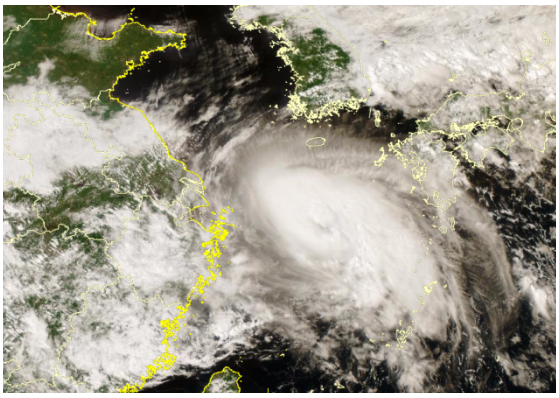

Fig. 1.10 (b) FY-4B Satellite image at 06:00UTC on 15th September.

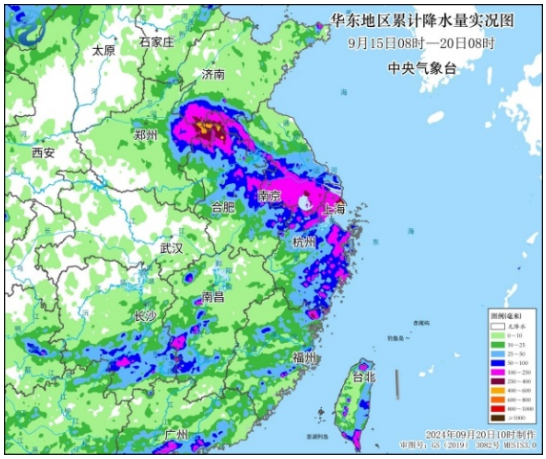

Fig. 1.10(c) Accumulated rainfall from 00:00UTC 15th to 00:00UTC 20th September

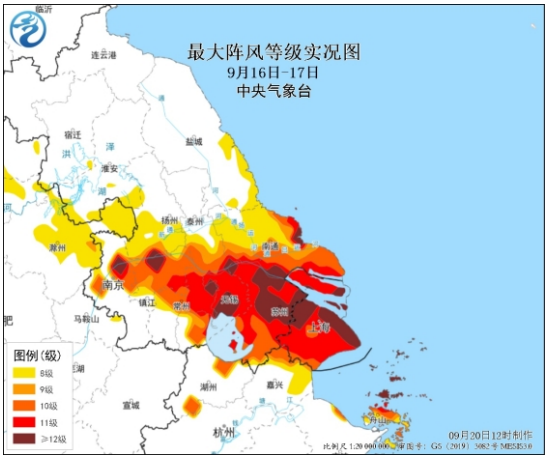

Fig. 1.10 (d) Maximum wind gust from 16th to 17th September

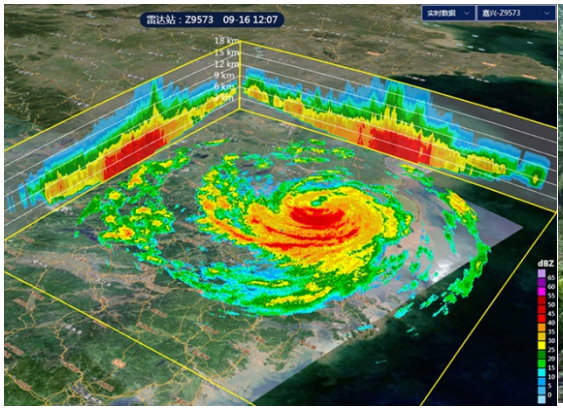

Fig. 1.10 (e) Radar echo image at 04:07UTC on 16th September

Fig. 1.10 (f) Disasters caused by Bebinca in Shanghai

A total of 918 flights in and out of the airport of Shanghai Pudong Airport and Hongqiao Airport were cancelled from the 15th to the 16th. All

highways within Shanghai were closed and controlled. Two people in Kunshan city died of electric shock due to wire detachment. All production operations at coastal ports in Zhejiang were halted. And 153 passenger ferry routes were suspended. Meanwhile, over 200 A-level tourist attractions closed. Highways in Jiangsu Suzhou, Nantong, Wuxi, Changzhou, Zhenjiang and some other areas were closed or speed limited. Six Yangtze River bridges also were closed. Serious urban waterlogging and farmland waterlogging occurred in Suzhou, Anhui Province.

6) Severe Tropical Storm PULASAN (2414)

Severe Tropical Storm Pulasan generated on the ocean near Guam at 12:00UTC on September 15th, then rapidly moved northwestward with a slow intensification. At 00:00UTC on the 19th, it strengthened into a severe tropical storm. At around 10:50UTC on the 19th, it made landfall as a strong tropical storm on the coast of Daishan County, Zhoushan, Zhejiang Province (25m/s, 990hPa). At around 13:45UTC on the same day, it made landfall again as a tropical storm on the coast of Fengxian District, Shanghai (23m/s, 995hPa).

After making landfall, Pulasan (2414) continued to move northwestward and moved into Jiangsu Province around 17:00UTC on the 19th, with its intensity continuing to weaken. Around 23:00UTC the same day, it weakened into a tropical depression and began to move

northeastward. Around 11:30UTC on the 20th, it moved from the southeast coast of Jiangsu into the southern Yellow Sea. Around 18:00UTC on the 20th, it strengthened to a tropical storm level and made landfall in South Korea. Then, it continued to move northeastward and gradually transformed into an extratropical cyclone.

Due to the impact of Pulasan (2414), heavy rain and rainfall successively occurred in Zhejiang, Shanghai, Jiangxi, Fujian, Jiangsu and other areas from 18th to 20th. Meanwhile, extremely heavy rainfall occurred in Pudong and Fengxian in Shanghai Province and Ningde in Fujian Province. The accumulative rainfall in some areas mentioned above reached 50~120mm, while it reached 150~379mm in some areas in eastern Shanghai, Nantong of Jiangsu Province, Taizhou of Zhejiang Province, Ningde of Fujian Province, and Ji'an of Jiangxi Province. During this period, gusts of Bft-8 to 9 and locally Bft-10 to 11 occurred along the coasts of Zhejiang, Fujian, Shanghai, and southern Jiangsu. On the afternoon of the 20th, a weak tornado appeared in Qingpu District, Shanghai.

About 335,000 people in Shanghai, Jiangsu, and Zhejiang Provinces were affected by Pulasan (2414) in different degree. The affected area of crops in Shanghai was 5.4 thousand hectares, with a direct economic loss of more than 30 million RMB. Fifty-four trains of Shanghai railway were suspended, and 26 ferry services were suspended. Schools were suspended in Pudong and Fengxian in Shanghai and Changzhou and Wuxi in Jiangsu

Province. On the 19th, 51 Flights in and out of the airport of Shanghai were cancelled and several scenic spots were temporarily closed in Hangzhou and Taizhou, Zhejiang Province. In addition, due to the continuously impact of Bebinca and Pulasan, the full fishing operation in the East China Sea originally scheduled for September 16th was postponed to September 20th.

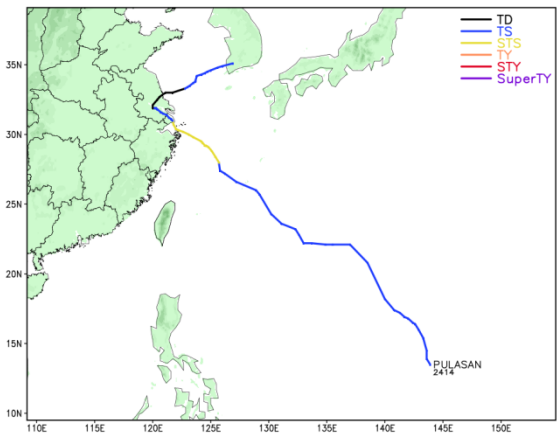

Fig 1.11 (a)Track of Pulasan (2414)

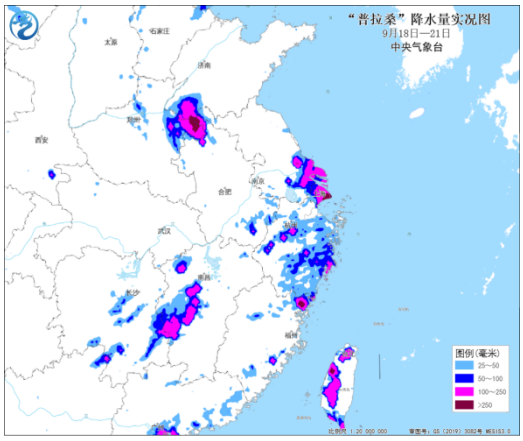

Fig 1.11 (b) Accumulated rainfall from 00:00UTC 18th to 00:00UTC 21th September

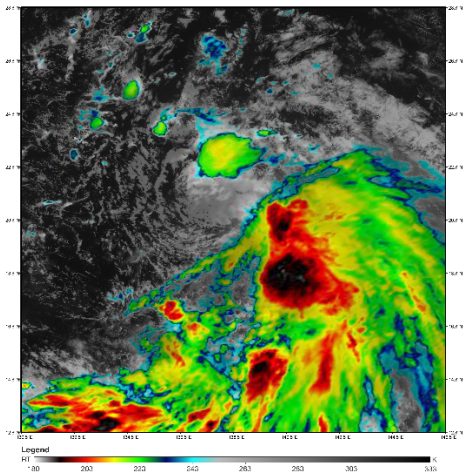

Fig. 1.11 (c) FY-4B Satellite image at 03:00UTC on 17th September

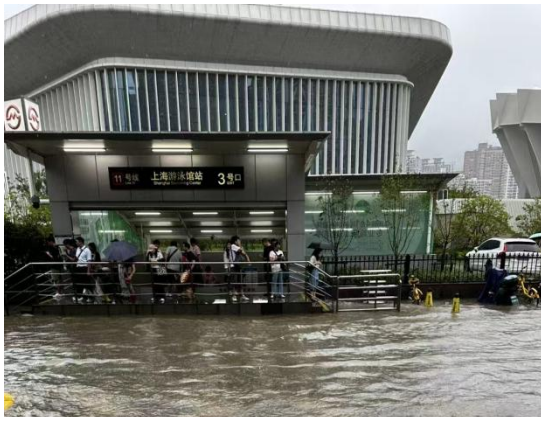

Fig. 1.11 (d) Disasters caused by Pulasan in Shanghai

7) Super Typhoon KRATHON (2418)

Super Typhoon Krathon generated over the open ocean to the east of the Philippines at 00:00UTC on 28th September. It moved in a northwesterly direction with rapidly increasing intensity. On the 29th, it moved into the Bashi Strait and strengthened to a super typhoon at 18:00UTC on the same day. On October 1st, it turned northward and then northeastward, with a slower speed and gradually weakened. On October 3rd at around 05:00UTC, it made landfall on the coast of Linyuan, Kaohsiung, Taiwan as a typhoon (38m/s, 965hPa). After landing, it still moved slowly and weakened into a tropical depression in the southwest of Taiwan Island around 18:00UTC on the 3rd.

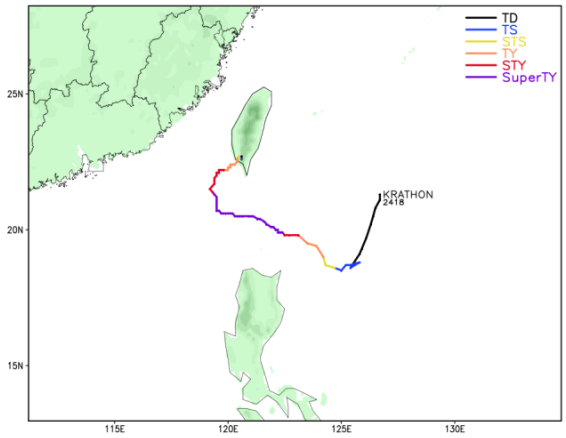

Fig 1.12 (a)Track of Krathon (2418)

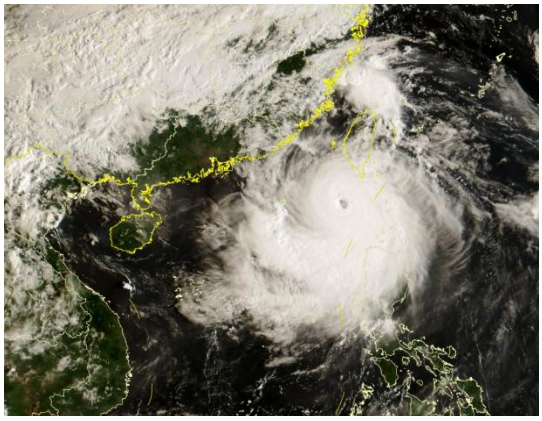

Fig. 1.12 (b) FY-4B Satellite image at 00:00UTC on 1st October

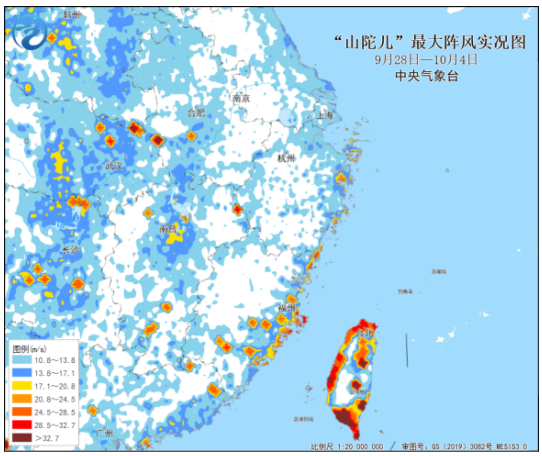

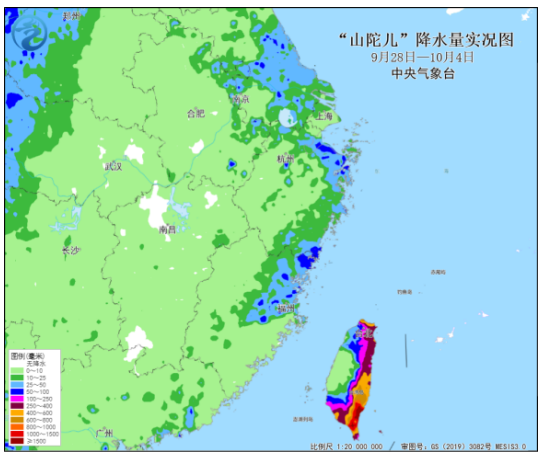

Fig. 1.12 (c) Maximum wind gust from 28th September to 4th October

Fig. 1.12 (d) Accumulated rainfall from 00:00UTC 28th September to 00:00UTC 4th October

Affected by Krathon (2418), from September 28th to October 4th, there were strong gusts of Bft-8 to 9 and locally Bft-10 to 11 along the coasts of Taiwan and Fujian Provinces. The southern coast of Taiwan experienced winds of Bft-10 to 12 and gusts of Bft-13 to 14. Under the complex influence of Krathon and cold air, extremely heavy rainfall occurred in the east and south of Taiwan Island, with the accumulated precipitation reaching 250~600mm, of which the southern part of Taiwan Island reached 1000~1500mm locally.

8) **Super Typhoon Trami (2420)**

Super TY Trami (2420) generated on the eastern ocean of the Philippines at 09:00UTC on October 21th, and gradually moved northwestward. Trami made its first landfall with intensity of STS (25 m/s, 985hPa) on the northeastern coast of Luzon around 17:00UTC on December 23th, before turning westward and moving into the central and eastern part of the SCS. It intensified into a severe tropical storm at 00:00UTC on December 25th, and a typhoon at 03:00UTC on December 26th. Around 02:40UTC on the 27th, it made second landfall with intensity of TS (23m/s, 990hPa) near the Hue border of Da Nang, Vietnam, and then weakened to a tropical depression. It remained inactive for a long time along the central and

eastern coasts of Vietnam, and the remnant circulation weakened further and returned to the SCS.

Affected by Trami (2420), Hainan Island had experienced the strongest rainstorm in the past decade from October 26th to 30th. The accumulative rainfall in city of Qionghai, Qiongzhong and Wanning exceeded 1000mm, with maximum over 1243.1mm in Huishan Town of Qionghai. The 24h accumulative rainfall at the three national meteorological observatories in Sanya, Ding 'an and Danzhou exceeded the historical maximum in October (Fig 1.13).

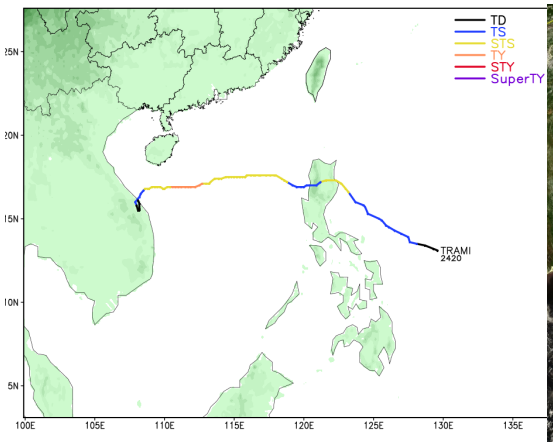

Fig 1.13 (a) Track of Trami (2420)

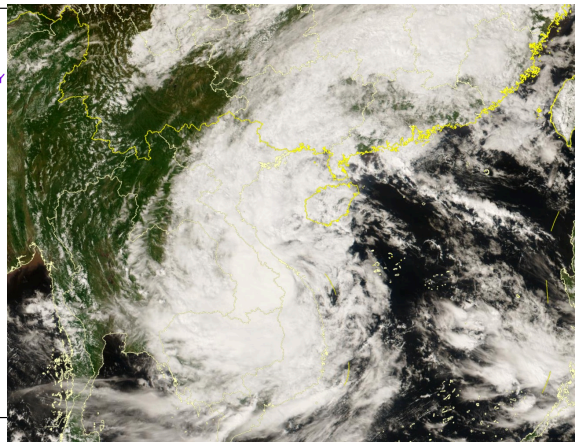

Fig. 1.13 (b) FY-4B Satellite image at 06:00UTC on 27th October

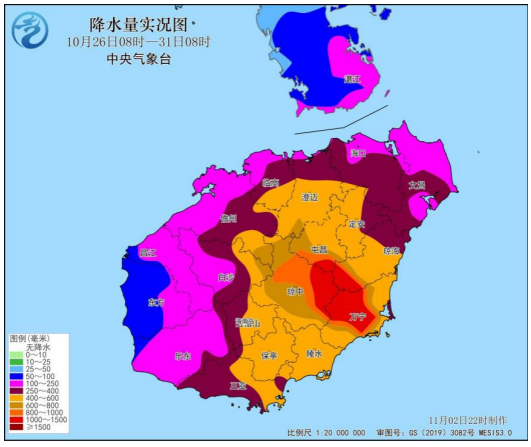

Fig. 1.13 (c) Accumulated rainfall from 00:00UTC 26th to 31th October

Fig. 1.13 (d) Disasters caused by Trami in Hainan

In Sanya, Haikou, Danzhou and other cities and counties of Hainan Province, 93,000 people were affected, 26,000 people were emergently evacuated and 2,000 hectares of crops were affected, with a direct economic loss of 230 million yuan. The continued discharge of water from the Niululing and Hongling reservoirs in Qionghai City, Hainan province, flooded villages along the Wanquan River, interrupted some power lines, blocked many roads and closed schools.

1.1.4 Climatic Prediction of TCs

In March and May, the National Climate Center carries out seasonal forecasts of tropical cyclones (TCs) in the South China Sea and the Northwest Pacific Ocean, including the number of TC generation, landfall frequency, possible track and intensity. The main methods are objective method of dynamic-statistical combination and physical mechanism diagnosis.

1) Annual Prediction of TCs

In March of 2024, it was predicted that the number of TCs generated in the South China Sea and the Northwest Pacific Ocean in 2024 would be 21-24, close to and less than the climatology (25, the average during 1991-2020, the same below). Among them, 6-8 TCs would land in China, close to the climatology (7), and the overall intensity of the landfall TCs would be strong. The tracks of the TCs would prevail westward and northwestward, with high possibility of northward influencing TCs.

2) Prediction of TCs during Boreal Summer

It was expected that there would be 7-9 TCs generated in the South China Sea and the Northwest Pacific Ocean in the summer of 2024, less than the climatology (11); the number of TCs landing in China would be 3-4, less than the climatology (4.7); the overall strength of typhoon would be weak; and the westward and northwestward tracks of typhoon activity would prevail, with high possibility of northward influencing TCs in midsummer.

Observation in summer shows that 8 TCs generated in the South China Sea and Northwest Pacific Ocean, with 3 of which landed in China, and weak in the overall intensity. The prediction of typhoon genesis and landfall frequencies, and overall intensity, and activity tracks, are all consistent with the observation. However, there is a certain deviation for forecasting the probability of the northward influencing typhoon compared to the observation with no typhoon tracks across north of 30°N, despite the observed Gaemi (2403) influencing the region of Northeast China.

1.2 Socio-Economic Assessment

By October 25th 2024, there are a total of 7 TCs that affected China. TC related disasters affected a total of 5.992 million people across 9 provinces, resulting in 8 fatalities. Additionally, 2.361 million people were urgently evacuated for safety, and 810,000 were relocated for emergency assistance. Over 1,400 buildings collapsed, and 49,000 buildings were damaged to varying degrees. The area of crops affected was 351,800 hectares, with a complete loss of 30,600 hectares.

Overall, the economic losses caused by typhoons in 2024 are less than those in the past decade, but the affected areas are concentrated and the affected areas are superimposed.

SuperTY Gaemi (2403) brought strong wind and rainfall to Fujian, Jiangxi and other places, and its residual circulation brought extreme heavy rainfall to Hunan, causing heavy losses. SuperTY Yagi (2411) which made landfall in early September, was the strongest typhoon that made landfall in China during autumn since meteorological records began. Under its influence, large areas in Hainan Island, southern Guangdong, and southern Guangxi experienced severe storms and heavy rainfall, causing widespread destruction. This resulted in 2.73 million people affected across Hainan, Guangdong, Guangxi, and Yunnan provinces, with 4 fatalities and the emergency relocation of 459,000 individuals.

In mid-September, Bebinca (2413) and Pulasan (2414) made landfall in East China successively, affecting 1.655 million people across Shanghai, Zhejiang, and Jiangsu provinces in varying degrees. There were 4 fatalities, and 114,000 people were urgently relocated, with over 6,000 buildings collapsing or being damaged.

At the end of October, although Trami (2420) did not make landfall in China, the extreme rainfall jointly caused by Trami and the cold air caused 10 deaths in Hainan Island.

Table.1 Landfall and impact TCs in China and related losses

TC Name (TC Num.)	Landfall Time and Location/ Intensity	Affected provinces	Affected population (10,000 persons)	Dead and missing population (person)	Population of emergency evacuation(10,000 persons)	Evacuated and relocated population (10,000 persons)
Maliksi (2402)	31th May 16:55 UTC Yangjiang, Guangdong/TS	Guangdong, Guangxi, Hainan	3.3	/	2.0	0.07
Gaemi (2403)	24th July 16:00 UTC Yilan, Taiwan/STY 25th July 11:50 UTC Putian, Fujian/TY	Zhejiang, Fujian, Jiangxi, Guangdong,Taiwan	156.3	/	47.9	23.4
Prapiroon (2404)	21th July 17:30 UTC Wanning, Hainan/STS	Guangdong, Guangxi, Hainan, Yunnan	1.1	/	0.7	0.3
Yagi (2411)	6th September 08:20 UTC Wenchang, Hainan/SuperTY 6th September 14:20 UTC Xuwen, Guangdong/SuperTY	Guangdong, Guangxi, Hainan	273	4	47.7	45.9
Bebinca (2413)	15th September 23:30 UTC Pudong, Shanghai/STY	Shanghai, Jiangsu, Zhejiang	130.2	4	104.3	10.8
Pulasan (2414)	19th Septemberr 10:50 UTC Zhoushan, Zhejiang/STS 19th September 13:45 UTC Fengxian, Shanghai/TS	Shanghai, Jiangsu, Zhejiang	35.3	/	33.4	0.6
Krathon (2418)	3rd October 05:00UTC Kaohsiung, Taiwan/TY	Taiwan，Fujian		5		
Trami (2420)		Hainan	55.9	10	6.3	3.9
Kong-Rey (2421)	31th October 0:00UTC Taitung Taiwan/STY	Taiwan, Fujian, Zhejiang, Shanghai	39.8	3	32.2	5.6
In Total			694.9	26	274.6	90.6

1.3 Regional Cooperation Assessment

1.3.1 The Senior Management and Operation Course on Tropical Cyclone Monitoring and Forecasting supported by CMA(2023)

From 20th November to 4th December, 2023, the Senior Management and Operation Course on Tropical Cyclone Monitoring and Forecasting for 2023, together with the 8th International Training Course on Tropical Cyclone Monitoring and Forecasting, was successfully held in Guangzhou, China.

This training course was co-organized by the Guangdong Meteorological Service and the China Meteorological Administration Training Centre (WMO Regional Training Centre-Beijing). A total of 35 participants from 33 countries and regions participated, representing all six WMO Regional Associations. Among them, 15 were meteorological officials at or above the division level, including two Directors-General of meteorological services/WMO Permanent Representatives (from Jordan and the Solomon Islands) and two department-level officials (Fig. 1.14).

The course covered topics such as Chinese practices in disaster prevention and mitigation, the latest WMO strategic development initiatives and the monitoring, forecasting, and early warning of tropical cyclones. This training also marked the official launch and use of the Guangdong-Hong Kong-Macao Greater Bay Area (GBA) branch of the

World Meteorological Center (WMC) Beijing for international training purposes.

Fig. 1.14 Closing ceremony of the Senior Management and Operation Course on Tropical Cyclone Monitoring and Forecasting in 2023.

1.3.2 The International workshop of "Parallel Analysis of Satellite Data in Operational Cyclone Monitoring"

The ESCAP/WMO Typhoon Committee's annual executive project "Parallel Analysis of Satellite Data in Operational Cyclone Monitoring" international workshop was successfully held in Shanghai from 29th to 30th May, 2024. This workshop focused on operational TC monitoring, aiming to enhance regional early warning capabilities based on multiple satellite data in strengthening international exchanges. A total of 12 overseas representatives from the meteorological departments of South Korea, Hong Kong, Macao, Thailand, the Philippines, Malaysia, and Vietnam, as well as nearly 10 domestic representatives from the National Meteorological Center (NMC), the National Satellite Meteorological Center (NSMC), and the Shanghai Meteorological Bureau, attended the two-day meeting. The

scientific sections specially invited several experts and researchers from the Korean Satellite Meteorological Center, the NSMC, the Nanjing Meteorological Innovation Research Institute of China Meteorological Academy, and Sun Yat-sen University to give keynote speeches and engage in panel discussions (Fig. 1.15).

Fig.1.15 Opening ceremony of the International workshop for
Parallel Analysis of Satellite Data in Operational Cyclone Monitoring

This successful workshop is conducive to enhancing the application effects of multi-source satellite data in precise typhoon monitoring, and proposing targeted application demonstration strategies for different satellite data. From the scientific discussion, it is important to strengthen regional cooperation in TCs monitoring, especially by promoting the application of Fengyun meteorological satellites in countries covered by the Typhoon Committee.

1.3.3 Progress of Tropical Cyclone Research and Review in 2024

Tropical Cyclone Research and Review (TCRR) journal mainly focuses on topics of tropical cyclone (TC) intensity and structure, TC genesis, TC precipitation, TC climatology, review of TC in history, operational TC forecast verification, TC induced storm surge and flood, and risk management etc. Quality of the TCRR journal is ensured by strict peer-review, with two-thirds of the reviewers are overseas experts. Authors come from 20 different countries and regions can finish the submission and peer-review through the ScholarOne system of Clarivate Analytics. Currently, TCRR is included in two full-text databases: ScienceDirect and DOAJ, in which all of the published papers are easily and freely available.

TCRR has published 51 issues since its launch in February 2012 through October 2024. In 2024, the journal hired Nanette Lomarda, a former senior official of the World Meteorological Organization, as the executive editor and selected 9 internationally renowned experts to join the journal's editorial board, greatly improving the operational efficiency and international influence of the journal.

TCRR was included in the Emerging Sources Index (ESCI) in 2017, so as a Web of Science Core Collection™ journal, TCRR received its first Journal Impact Factor (JIF)™ of 2.4 in 2024. It was ranked 66 out of 110 (Q3) in the JCR Meteorology & Atmospheric Sciences category. And TCRR was included in Scopus at the end of 2022, so it also received its

first CiteScore of 4.6 in 2024. It was ranked in Q2 in three categories (26 out of 109 in Safety Research, 84 out of 324 in Modeling and Simulation, and 26 out of 73 in Computers in Earth Sciences).

II. Summary of Progress in Priorities supporting Key Research Areas

2.1 Application and Evaluation of AI Weather Models in Tropical Cyclone Forecast

2.1.1 New AI Weather Forecast Model Fengqing

Following the international advances in artificial intelligence meteorological large models, together with Tsinghua University, National Meteorological Centre (NMC) developed a large AI weather forecast model based on the AI technology and meteorological Physical mechanisms named Fengqing. With the strong physical representation, the Fengqing model has the strong physical infusion and interpretability. Transforming the multi-scale spatial-temporal interaction of the atmosphere into a state transition in the hidden space ensures efficient computation while providing physical interpretability for prediction results.

In terms of training strategy, energy conservation iterative training is carried out for short and medium range prediction. The model taken into account the physical conservation characteristics during the training process. By constructing a Hamiltonian conservation system on the coarse grid meteorological reality analysis, potential conservation properties in the meteorological process are explored. And based on this, the conservation properties of the model forecast results are constrained. This

effectively improves the capability of long-term forecast and the forecast performance for severe weather.

Besides, the model adopts an extensible multi time optimization strategy, which separates the calculation of parameter gradients for each time period and then optimizes them uniformly, reducing the cumulative error during the iteration process and improving the short- and medium-term forecasting performance. In addition, the NMC has actively introduced the Fengwu-TC typhoon intensity forecast model from the Shanghai Artificial Intelligence Laboratory.

In addition, integrating 7 large AI weather forecast models including Fengqing, Pangu, Fengwu, Fuxi, GraphCast, FourCastNet, and AIFS, NMC developed a comprehensive typhoon and marine forecasting and analysis platform. This platform can display and compare the forecasted situation field, typhoon track, and intensity of each model, and provide real-time forecast verification from multiple angles for forecasters to analyze and reference.

2.1.2 AI-Drived Typhoon Forecasting System Completes First Real-Time Forecast

During the activity of this year's Typhoon Gaemi (2403) and Typhoon Prapiroon (2404), the high-resolution typhoon forecasting system driven by a large-scale AI weather model (hereafter referred to as AI-TRANS),

jointly developed by the Chinese Academy of Meteorological Sciences and the National Meteorological Center, completed its first real-time forecast. Verification indicates that AI-TRANS can operate stably within the current operational environment of the China Meteorological Administration, providing real-time, high-resolution (2km) forecasts for the entire life cycle of typhoons in the Northwest Pacific and South China Sea. AI-TRANS demonstrated excellent forecasting capabilities in terms of typhoon track, intensity, structure, and detailed wind and rainfall predictions, showing significant potential for operational application. This will provide strong technical support for the operational upgrade of the TRANSv1.0, which is currently operational and led by the Chinese Academy of Meteorological Sciences.

The AI-TRANS system successfully forecasted the northwestward track of Typhoon Gaemi this year, particularly capturing the looping motion east of Taiwan Island. Notably, several major global and regional models, as well as subjective forecasts from forecasters, did not predict this looping motion. However, the AI-TRANS system was able to accurately forecast this motion (see Fig. 2.1, bottom-left inset).

Priority Areas Addressed:

Meteorology

- Enhance the capacity to monitor and forecast typhoon activities particularly in genesis, intensity and structure change.
- Develop and enhance typhoon analysis and forecast techniques from nowcasting to medium-range, and seasonal to long-range prediction.

Contact Information:

Member: China

Name of contact for this item: Nie Gaozhen

Telephone: +86-010-58995842

Email: niegaozhen@cma.gov.cn

Name of contact for this item: Xiu Hongxiong

Telephone: +86-010-68409884

Email: xuhx@cma.gov.cn

2.2 Advances in Numerical Modeling of Tropical Cyclone

2.2.1 Optimization and Improvement of Global Model Numerical Forecasting System CMA-GFS 4.0

In order to improve the overall forecast performance of CMA-GFS 4.0 for typhoons and to address a series of problems that the traditional convective parameterization scheme is not suitable for high-resolution models, the CMA-GFS convective parameterization scheme is optimized and improved. The specific measures include firstly, increasing cloud roll out and compensating subsidence items, supplementing sub grid convective cloud amount feedback, and meeting the requirements of CMA-GFS for cloud amount explicit prediction. Secondly, the influence of the relative humidity of the sub cloud layer on the sub grid convection trigger is introduced to reasonably reduce the excessive sub grid convection trigger frequency. Thirdly, the cloud bottom mass flux diagnosis is optimized by using the diagnostic equation of sub grid convection rising velocity, which solves the problem that the high-resolution model no longer meets the quasi-equilibrium assumption in the convective scheme, and enhances the triggered sub grid convective intensity. Finally, adjust the rainwater conversion coefficient, reasonably reduce convective precipitation conversion and increase high cloud roll out. At the same time, the advective scheme of cloud amount, cloud physical water matter and the treatment of boundary layer top layer cloud are optimized.

The improvement of the physical process of the model has systematically improved the prediction performance of CMA-GFS for weather situation, heavy rainfall and tropical cyclone. 87 back calculation tests from July to August 2023 showed that the average track error of tropical cyclone in 1-5 days decreased by 2.67% -10.04% while the improvement for intensity forecast is not obvious.

2.2.2 Improvement of 25km Global Ensemble Forecast Disturbance Technology and System Integration

2.2.2.1 Improving the Calculation Technology of Tropical Cyclone Singular Vector

Based on the original tropical cyclone target area singular vector (TC-SV) calculation scheme in the Western North Pacific and the North Indian Ocean, the TC-SV calculation module for other basins is added, and the setting of TC-SV target area range is optimized to realize the adaptive setting and calculation function of TC-SV target area in global ocean. Taking the case of multiple typhoons in the global waters as an example, the 25km ensemble prediction test of the original TC-SV scheme and the new TC-SV scheme for the global waters was carried out.

The results show that the structure of SV in each target area obtained by the new TC-SV calculation scheme is reasonable, the tropical cyclone

track and intensity prediction results in the Western North Pacific are similar to those in the original scheme, and the tropical cyclone track and intensity prediction in other basins are reasonable. Meanwhile, the CMA-GEPS with 25km resolution and new TC-SV scheme has better track and intensity prediction compared with the CMA-GEPS with 50km resolution.

2.2.2.2 Improved Initial Perturbation Technique

Based on the CMA global/regional ensemble forecasting system initial value perturbation technology integration framework, for the application of global ensemble forecasting, a multi-scale singular vector initial value perturbation scheme based on two scales (2.5 degrees large-scale singular vector and 1.5 degrees mesoscale singular vector) is adopted. In order to solve the problem of insufficient initial value disturbance of global ensemble prediction in tropical areas, the ensemble data assimilation EDA disturbance is introduced into the initial value disturbance of global ensemble prediction, and the initial value disturbance scheme of mixed EDA and singular vector is constructed. The ensemble prediction experiments of different initial value disturbance schemes were carried out. The experimental results show that the combination of EDA and singular vector initial value scheme can significantly improve the ensemble dispersion and probability prediction skills of various forecasts in the

tropical region, and it can improve the 24-hour cumulative precipitation probability prediction skills in China.

2.2.2.3 Improved SPPT Scheme for Stochastic Perturbation of Model Physical Process

The original SPPT scheme used a random type representing a single weather scale. In order to reflect the characteristics of the model physical process error on different scales, the random type characteristics of the SPPT scheme were improved. The random types of three spatial scales (representing mesoscale, weather scale and planetary scale) were linearly superimposed to generate a random type including multi-scale information, which was applied to the SPPT to construct a multi-scale SPPT scheme. A 25km ensemble prediction experiment using multi-scale SPPT scheme is carried out. The results show that the new scheme improves the dispersion and prediction skills compared with the original single-scale SPPT scheme in the tropical region.

2.2.3 Research and Development of New Version of CMA-TYM

The Earth System Modeling and Prediction Center of China Meteorological Administration developed a regional mesoscale Assimilation Prediction System (CMA-MESO6.0) with 1km/1h high spatial and temporal resolution covering China and the offshore region in

2023. The system has been optimized and improved in the dynamic framework and physical process, and abundant parallel optimization has been carried out to improve the computational efficiency. At present, the 1km/1h regional mesoscale assimilation prediction system has been running in real time.

In 2024, The Earth System Modeling and Prediction Center of China Meteorological Administration carried out the research and development of the new version of CMA-TYM based on CMA-MESO 6.0. It mainly includes upgrading the basic version of CMA-TYM to CMA-MESO 6.0, the vertical layer L71 of CMA-MESO 6.0 is used to replace the 68 layers of the original operational system, the physical process is further optimized by adding dissipative heating parameterization and terrain turbulence drag parameterization. The horizontal resolution of the new version of CMA-TYM is still 9km. Based on the new version, the main tropical cyclone back calculation in 2023 was completed, and the results showed that the new version CMA-TYM significantly reduced the average track and intensity prediction errors (Fig. 2.2).

2.2.4 Technology Upgrade and Operation of CMA-TRAMS

The overall performance of CMA-TRAMS in 2024 was stable. Up to 18th October, 19 typhoons had been successfully forecasted. Verification showed that, the 24h, 48h and 72h track forecast errors of CMA-TRAMS

were 59.2km, 114.2km, and 182.4km, respectively. and the intensity forecast errors were 9.1hPa, 11.6hPa, and 12.9hPa, respectively. The complexity of the typhoon situations in 2024 had led to a slight increase in track forecast errors, especially for the Typhoon Yagi with a notable forecast deviation. From 12:00UTC on September 1st to 00:00UTC on September 3rd, the forecast track of Typhoon Yagi near Luzon was close to the actual situation. However, after entering the South China Sea, the CMA-TRAMS predicted that Typhoon Yagi would make landfall in the Pearl River Delta region, which showed significant discrepancies. The forecasts were adjusted after 12:00UTC on September 3rd. A review of the forecast problems associated with Typhoon Yagi revealed that the convective trigger function in the parameterization scheme had a significant influence on typhoon forecast, especially on long lead time. Based on five sets of comparative tests with different trigger functions, an improved convective trigger function in the parameterization scheme was carried out. The improved scheme proved an effective method of alleviating the forecasting challenges associated with Typhoon Yagi. As shown in Figure 2.3, the results of the back-calculations of 2024 demonstrated that the overall evaluation of the improved scheme yielded positive outcomes. At present, scheme sch4 has been applied to the improved version.

Priority Areas Addressed:

Meteorology

- Enhance the capacity to monitor and forecast typhoon activities particularly in genesis, intensity and structure change.
- Develop and enhance typhoon analysis and forecast technique from short- to long-term.

Contact Information:

Member: China

Name of contact for this item: Ma Suhong

Telephone: +86-010-68400467

Email: mash@cma.gov.cn

Name of contact for this item: Zhang Xubin

Telephone: +86-020-39456428

Email: xbzhang@gd121.cn

2.3 Tropical Cyclone Observation Experiment

2.3.1 Jointly Multi-aircrafts observations for Typhoon Prapiroon

On July 21, 2024, in accordance with the relevant requirements for the trial operation of the national mobile observation service, under the unified deployment of the China Meteorological Administration(CMA), the CMA Meteorological Observation Centre (MOC), together with the Hong Kong Observatory(HKO), Hainan Provincial Meteorological Bureau, Guangzhou Institute of Tropical and Marine Meteorology, CMA Earth System Modeling and Prediction Center and other units, carried out several joint observations of multi-aircraft platforms (Haiyan type I UAV and man-machine) in the sensitive areas and main covered areas of Typhoon Prapiroon(2404), and accurately captured the cloud structure of Prapiroon. These precious observation data can help build the first line of defense for meteorological disaster prevention and reduction.

At 2:45UTC 21th July, a Haiyan I UAV equipped with airborne dropsonde, temperature and humidity profiler and cloud radar took off from Boao Airport in Hainan province to carry out a mobile observation mission of Typhoon Prapiroon. It landed safely at Boao Airport at 4:45UTC. The flight lasted two hours. At 10:00 UTC on the same day, a manned aircraft belonging to the Hong Kong Observatory and the Hong Kong Flying Service conducted observations in its airspace. The aircraft carried a drop sonde and made drop observations during the flight. During

the flight of Haiyan I UAV, a total of eight sondes were launched (Fig. 2.2a) and 4893 valid observations were obtained. The nearest sonde delivery point was only 68.8km from the typhoon center. During the flight, all the observed data were transmitted in real time. The observation data obtained in real time and the MICAPS products generated from the data were distributed to the Guangdong Tropical Research Institute, Shanghai Typhoon Research Institute, CMA Earth System Modeling and Prediction Center and other operation centers for application. Preliminary evaluation results show that the delay of all products is about 15 minutes. According to the data assimilation experiment conducted by Guangdong Tropical Research Institute based on CMA-TRAMS model, the forecast track of typhoon Prapiroon predicted by CMA-TRAMS model is closer to the reality after assimilating the observation data of UAV, while the forecast track without assimilating observation data is farther west than the real typhoon track. The 48h track error decreases from 94km to 38km, and the 66h error decreases from 142km to 100km. In addition, the assimilated observation data also improved the precipitation forecasting ability of the model. In other words, not only was the TS score improved overall, but especially over 50mm precipitation, the TS score increased from 0.28 to 0.38 for 12-36h leading time and from 0.32 to 0.4 for 24-48h leading time (Fig. 2.2b).

The joint mobile observation provided direct observation data support for the forecast of typhoon track and intensity. At the same time, the joint observation experiment is of landmark significance to promote the construction of the mobile typhoon observation system in the South China Sea, better play the service effect of typhoon monitoring and forecasting, and build a strong first line of defense for disaster prevention and reduction.

2.3.2 TC Field Observation Experiments in 2024

From March to June in 2024, based on the observational requirements of related research and operational work, a field scientific experiment plan for typhoons in 2024 was formulated. The plan focuses on the wind field and cloud physical structure of typhoons to promote the integration of typhoon observation and forecasting. The observational part of the observation-forecast integration technical plan was completed, and an observation-forecast integration scheme operational process was established. This aims to achieve seamless integration of field observation, data transmission, data assimilation, and model forecasting, in order to promote the timely and effective application of 2024 observational data in model assimilation.

From July to September 2024, leveraging the East China Typhoon Observation Network of the CMA-STI, a collaborative effort was undertaken with meteorological bureaus from various provinces and cities

in East China, the University of Science and Technology of China, and several instrument manufacturers. This joint operation targeted key scientific and operational issues such as the intensity forecast of offshore typhoons and the microphysical mechanisms of heavy rainfall. Observations were conducted on typhoons Gaemi and Bebinca using a combination of fixed stations and mobile observation equipment. The initiative aimed to collect real-time observational data and integrate it into operational models for assimilation and forecasting experiments. The objective was to explore and implement an integrated process from the identification of typhoon observation sensitive areas, through the implementation of typhoon observation operational trials, to the assimilation of multi-source typhoon observation data, application in model forecasting, and ultimately, effectiveness assessment. This approach was designed to enhance the seamless integration of field observations, data transmission, data assimilation, and model forecasting, thereby promoting the timely and effective application of observational data in model assimilation for the year 2024 (Fig. 2.3).

Priority Areas Addressed:

Meteorology

- Enhance the capacity to monitor and forecast typhoon activities particularly in genesis, intensity and structure change.

Contact Information:

Member: China

Name of contact for this item: Zhu Xuesong

Telephone: +86-021-54896126

Email: zhuxs@typhoon.org.cn

Name of contact for this item: Sun Xia

Telephone: +86-010-58994375

Email: sunxia063@126.com

2.4 Comprehensive Collaborative Observation Experiment for Typhoons in the South China Sea

From July to September 2024, the China Meteorological Administration organized a comprehensive and coordinated typhoon observation experiment in the South China Sea. The tests were conducted in and around the South China Sea. The basis of the observation test includes Fengyun meteorological satellite monitoring network, large unmanned aerial vehicle mobile observation service, manned aircraft crossing typhoon observation, Beidou navigation flat drift sounding service and the South China Sea meteorological observation network. The experiment focused on four aspects: first, observing peripheral atmospheric circulation using satellites, soundings, and ocean observation equipment; second, investigating the internal structure of typhoons through aircraft penetration, downward soundings, and intensified satellite observations; third, examining air-sea interaction using underwater gliders, buoys, and integrated marine platforms; and fourth, analyzing the fine structure and key physical processes of landfall typhoons with multi-band radar, wind profilers, and raindrop spectrometers. The experiment will deepen understanding of the multi-scale structural characteristics of the air-sea interface in the context of South China Sea typhoons, as well as the three-dimensional internal structure, cloud microphysics, boundary layer features, and their evolution processes. During the experiment, valuable

observational data were successfully collected regarding Typhoon Prapiroon (2404) and Typhoon Yagi (2411) as they impacted the South China Sea (Fig. 2.6).

Priority Areas Addressed:

Meteorology

- Enhance the capacity to monitor and forecast typhoon activities particularly in genesis, intensity and structure change.

Contact Information:

Member: China

Name of contact for this item: Zhang Xubin

Telephone: +86-020-39456428

Email: xbzhang@gd121.cn

2.5 Applications of Fengyun Satellites in Tropical Cyclone Operation and Research

2.5.1 Improved Applications of Fengyun Series Satellite Service Platform and Products

The "Fengyun Earth Satellite Meteorological Service Platform" developed by the National Satellite Meteorological Center was put into operation, with integrated observation data including FY-4B geostationary meteorological satellite, FY-3E satellite, etc., fully utilizing the different characteristics of satellite channels (Fig.2.7). During the activities of typhoons Gaemi (2403), Yagi (2411), Bebinca (2413) and Pulasan (2414), the large-scale background could be revealed by the middle- to upper-level water vapor images, and the detailed structural characteristics of the typhoon eyewall and spiral rainbands could be monitored using true color (visible) imageries. The platform provides 250-m fine-scale observations in 1-minute intervals, AI-based FY-4B precipitation estimation, automatic identification of convections, surface wind recognition, cloud-derived-wind, integrated sea surface temperature, subtropical high detection etc., which can support the entire lifespan of typhoons. Several products are developed, such as convective activity intensity index by using combined channel 1.3μm and 1.6μm data, radial averaged brightness temperature Hovmoller diagram based on FY-4B, AI-based QPE product using Geo High-speed Imager, integrated SST on FY-3D/E/F satellite. In Typhoons

Yagi (2411) and Bebinca (2413), the wind speed from FY-3E WindRAD and precipitation from FY-3G PMR contribute to the TC monitoring.

2.5.2 FY-4B GIIRS Enhanced Observations

In response to Super Typhoons Gaemi (2403) and Yagi (2411), the FY-4B GIIRS initiated enhanced observations (Fig. 2.8) at 05:00UTC on July 24th and at 00:00UTC on September 5th, 2024, with a temporal resolution of 15 minutes.

Control experiment and the GIIRS assimilation experiment are carried out to evaluate the function of FY-4B GIIRS target observations on the forecasting. Figure 2.9 shows the diagnostic results of the typhoon track forecasts from four assimilation experiments for Gaemi (2403). In the early stages of the forecast, the track forecasts of the two sets of experiments almost coincide within the 18-h forecast period. After forecasting for 24h, the differences between the two sets of experiments gradually increase. After 60-h of forecasting, compared to the control experiment, the typhoon track forecast after GIIRS assimilation is significantly closer to the real track. The four initial forecast experiments improved the average typhoon track forecast error by 17.66%, 27.05%, 27.5%, and 10.68%, respectively. The diagnostic results of track forecasts in the assimilation experiment for Yagi (2411, Fig.10) is different from Gaemi (2403), the overall impact of GIIRS assimilation on the forecast of Yagi (2411) is relatively small, with

the five forecast experiments leading to average improvements in TC track forecasts of 11.08%, -1.28% (negative contribution), 0.55%, 8.94%, and 7.65%, respectively.

Priority Areas Addressed:

Meteorology

- Enhance the capacity to monitor and forecast typhoon activities particularly in genesis, intensity and structure change.
- Develop and enhance typhoon analysis and forecast technique from short- to long-term.

Contact Information:

Member: China

Name of contact for this item: Song Wanjiao

Telephone: +86-010-58995547

Email: songwj@cma.gov.cn

Name of contact for this item: Ma Suhong

Telephone: +86-010-68400467

Email: mash@cma.gov.cn

2.6 Advances in Tropical Cyclone Scientific Research

2.6.1 Changes and Uncertainties in Projections of the Tropical Cyclone Genesis Under Different Warming Scenarios in the Future

Reliable projections of tropical cyclone (TC) activities in the western North Pacific (WNP) are crucial for climate policy-making in densely-populated coastal Asia. Existing projections, however, exhibit considerable uncertainties with unclear sources. Here, based on future projections by the latest Coupled Model Intercomparison Project Phase 6 climate models, we identify a new and prevailing source of uncertainty arising from different TC identification schemes. Notable differences in projections of detected TCs and empirical genesis potential indices (GPIs) are found to be caused by inconsistent changes in dynamic and thermodynamic environmental factors affecting TC formations. While model uncertainty holds the secondary importance, we show large potential in reducing it through improved model simulations of present-day TC characteristics. Internal variability noticeably impacts near-term projections of the WNP tropical cyclogenesis, while the relative contribution of scenario uncertainty remains small. Our findings provide valuable insights into model development and TC projections, thereby aiding in adaptation decisions (Fig. 2.11).

2.6.2 Research on Downscaling Complex Terrain Wind Fields Based on Deep Learning

In complex terrain areas, deep learning is used to develop the multi-correlation fusion downscaling technology of adaptive areas. Through the intelligent module fusion of wind field, topographic grid data and observation data, the high-precision downscaling of the near-surface wind field under complex terrain is achieved. A near-surface wind downscaling method for a complex terrain region is proposed, named TerraWind based on deep learning that can synthesize wind-terrain correlations and inter-station correlations, and adapt to different geographic regions and station densities. Experimental results in Eastern China demonstrate that TerraWind reduces wind speed Mean Absolute Error (MAE) and Root Mean Square Error (RMSE) by an average of 42.6% and 33.3%, respectively, compared to three interpolation methods. Furthermore, TerraWind achieves an average reduction of 35.3% in wind speed MAE and 25.6% in wind speed RMSE compared to four deep learning models (Table 2.1).

2.6.3 Observational and Mechanism Analysis on High-Impact Typhoon Doksuri(2305)

High-impact typhoon Doksuri (2305) made landfall in China as a severe typhoon and brought extreme rainfall and severe damage as its

remnant revived after its landfall. The fine-scale track, intensity, and structural evolution of Doksuri (2305) is comprehensively analyzed by combining multi-source observations including satellite, space-borne synthetic aperture radars (SAR), weather radars and *in situ* observations of buoys. The results show that Doksuri (2305) experienced secondary eyewall formation (SEF), concentric eyewall maintenance (CEM), and eyewall replacement cycle (ERC) processes when entering the South China Sea and prior to landfall. The variations in the track and intensity of Doksuri are closely correlated with the fine-scale evolution of its structure (Fig. 2.12).

Furthermore, the revival mechanism of Typhoon Doksuri (2305) remnant after landfall is extensively explored. The remnants vortex of Doksuri sustained an inland trajectory for 3 days. Based on multi-source observations and ERA5 reanalysis data, by calculation of moist potential vorticity and analysis of slantwise vorticity development (SVD), Doksuri remnants transported sufficient moisture in the mid-lower troposphere while maintaining a significant warm-core structure over the course of maintenance and revival, which intensified the north-south temperature and humidity gradients, causing tilting of the isentropic surfaces remarkably. According to the SVD theory, the tilting gave rise to vorticity development and forced upward air motion on the northern side of the remnant vortex. Moreover, numerical sensitivity experiments based on the

WRF model reveal that the topography of Taihang Mountains and the diabatic heating associated with surface and convective latent heat fluxes also played an important role in the revival of the Doksuri remnants. The dynamic and thermodynamic mechanisms derived by this study will help improve prediction and early warning of the disasters induced by TC remnants.

The effect of anthropogenic warming on "23·7" extreme rainfall event related to Doksuri (2305) in the Beijing–Tianjin–Hebei region is analyzed using ensemble convective-permitting simulations. Two sub-regions with opposite responses are identified: anthropogenic warming decreased (increased) precipitation in the northern (southern) sub-region of the Beijing–Tianjin–Hebei area. Further analysis shows that anthropogenic warming intensified the remnant of Typhoon Doksuri (2305) and increased rainfall in its inner core, but decreased rainfall in the peripheral spiral rain band. These are the main reasons for the locally inconsistent responses of extreme rainfall to anthropogenic warming. We emphasize that anthropogenic warming, as a global background signal, directly affects the intensity and structure of specific weather systems rather than local precipitation. A high-impact extreme rainfall event therefore cannot always be simply attributed to climate warming enhancing precipitation at every location in a particular region.

2.6.4 The Impact of Assimilating X-band Phased Array Radar Radial Wind Observations on the Forecast of Tropical Cyclone Saola(2309)

X-band phased array radar (XPAR), a promising new instrument to detect fine structure of severe weather conditions, has recently been deployed at numerous locations across China. However, the impacts of assimilating its observations on tropical cyclones (TCs) remain unclear. This study investigates the effects of assimilating XPAR radial wind velocity observations, both alone and in combination with S-band Doppler radar radial winds, for TC Saola (2309). Compared to experiment assimilating only S-band radar data, the use of XPAR observations significantly reduces TC intensity error, with maximum reduction of 9.3m/s for XPAR observations alone and 10.3m/s for combined dataset, while also improving track forecasts. Assimilating XPAR observations successfully enhances the circulation and thermodynamic structure of the TC compared to the assimilation of S-band radar observations, addressing the weakening of the eyewall wind speed caused by terrain effects. Additionally, the spiral rainbands are better captured when XPAR observations are included, particularly in the combined experiment. The structure improvement finally leads to an enhancement of precipitation forecast skill, especially for extreme rainfall. These improvements are attributed to XPAR's capability to provide more accurate observations of the TC’s lower-layer inner core (Fig. 2.13).

2.6.5 The impact of the Northeast China Cold Vortex on TC track and Intensity in China

The Northeast China cold vortex(NCCV) and tropical cyclone(TC) are two important cyclonic systems over eastern Asia, characterized by wide coverage, long duration, and deep vertical stretching. The NCCV can be recognized as a frequent upper-level system influencing TC behavior, as the active time of NCCVs overlaps with the TC seasons. The impact of NCCV on TC track and intensity is studied based on statistics.

There is a significant inverse relationship between the NCCV during June–September and simultaneous northward-moving TCs during 1981–2021. Fewer (more) northward-moving TCs are observed during NCCV active (inactive) year a combination of less (more) TC genesis, particularly over the central Pacific region of 10–30°N and 130–150°E, and fewer (more) northward-moving TCs moving northwestward and making landfall in coastal regions of the Yellow Sea and Bohai Sea. These regions are characterized by significantly decreased low-level vorticity and mid-level humidity, which impedes TC genesis and notably enhances the deep-layer subtropical straight westerly steering flow, thus blocking the northward movement of TCs. These remarkable environmental changes during different NCCV years are clearly linked with the changes of an anomalous anticyclone in the subtropics. In short, more (less) NCCV

activity strengthens (weakens) the anomalous anticyclone, resulting in fewer (more) northward-moving TCs.

There is a significant decrease in the rate of TC weakening and a lower probability of rapid weakening (RW) in the environments of NCCVs. This is mainly attributable to the external dynamic forcing induced by the NCCV as the eddy angular momentum import at upper levels increases significantly, which offsets the unfavorable decrease in sea surface temperature and increase in vertical wind shear. The upper-level positive potential vorticity anomaly band from the NCCV involves into the TC circulation from the southwestern quadrant, helping the development of convections triggered in the downshear right side of the TC. These results elucidate a fundamental relationship between TCs and NCCVs, and the findings contribute to a deeper comprehension of TC behavior under the influence of NCCVs.

2.6.6 Improvement of Typhoon Extreme Precipitation Forecasting in North China by Pangu-Weather AI-Driven Regional WRF Model

In the realm of weather forecasting, the implementation of Artificial Intelligence (AI) represents a transformative approach. However, AI weather forecasting method still faces challenges in accurately predicting meso- and smaller-scale processes and failing to directly capture extreme precipitation due to regression algorithm's nature, coarse resolution, and

limitations in key variables like precipitation. Therefore, we propose a state-of-the-art technology which integrates the strengths of the Pangu-Weather AI weather forecasting with the traditional regional weather model, focusing specifically on enhancing the prediction of extreme precipitation events, as mainly exemplified by an unprecedented precipitation in North China from 29 July to 1 August 2023, and an additional extraordinary precipitation event as a supplementary validation to further ensure the accuracy of this technology. The results show that the AI-driven approach exhibits superior performance in capturing the spatial and temporal dynamics of extreme precipitation events (Fig.2.14). Remarkably, with a threshold of 400 mm, the AI-driven model secures a Threat Score (TS) of 0.1 for forecast lead time reaching up to 8.5 days (Fig.2.15). This performance notably surpasses the performance of traditional GFS-Driven models, which achieve a similar TS only within a limited 3-day forecast lead time. This considerable enhancement in forecast accuracy, especially over extended lead times illustrates the AI-driven model's potential to advance in long-term forecasts of extreme precipitation, previously considered challenging, emphasizing the potential of AI in augmenting and refining traditional weather prediction.

Priority Areas Addressed:

Meteorology

- Enhance the capacity to monitor and forecast typhoon activities particularly in genesis, intensity and structure change.
- Develop and enhance typhoon analysis and forecast technique from short- to long-term.

Contact Information:

Member: China

Name of contact for this item: Zhu Xuesong

Telephone: +86-021-54896126

Email: zhuxs@typhoon.org.cn

Name of contact for this item: Li Ying

Telephone: +86-010-58995830

Email: yli@cma.gov.cn

Name of contact for this item: Xiu Hongxiong

Telephone: +86-010-68409884

Email: xuhx@cma.gov.cn

Name of contact for this item: Wang Qian

Telephone: +86-010-58995840

Email: qianwang@cma.gov.cn

2.7 Improvement of Typhoon-related Disaster Management

2.7.1 Typhoon Disasters, Comprehensive Impact of Wind and Rain, and Disaster Prevention and Reduction Achievements in China in 2023

Using data from meteorological observation stations, the Ministry of Emergency Management, and the Yearbook of Tropical Cyclones in the Northwest Pacific, it has been found that the typhoon disaster loss indicators for 2023 are below the 40-year average and roughly equal to the 10-year average. Although typhoons in 2023 brought multiple episodes of extreme heavy rainfall, with rainfall in many stations breaking historical maximum precipitation records, both the wind impact index and the comprehensive wind-rain impact index were lower than the averages for both the 40-year and 10-year periods. Furthermore, in 2023, typhoon disaster prevention and mitigation measures were remarkably effective. Advanced technologies supported the accurately forecast for the heavy rainfall areas of typhoons such as Doksuri, and the defense response was implemented on time, successfully avoided various secondary disasters. The implementation of disaster prevention and mitigation work was also a key factor in the lower typhoon disaster losses in 2023 (Fig. 2.16).

2.7.2 Analysis of Typhoon Disaster and Wind and Rain Impact in Different Provinces of China from 2014 to 2023

The disaster loss indicators in the Southern China generally show a downward trend, while there is a certain upward trend in the Northern China. The decrease in the number of affected people in the South China area is the most significant, with a decrease rate of 1.378 million people/year, while the Northeast China and the Inner Mongolia Autonomous Region show an upward trend, among which Heilongjiang and Jilin's affected population increase rate exceeds 50,000 people/year. Similar to the trend of affected people, the disaster situation of crops in the Northeast region and Inner Mongolia Autonomous Region shows a certain upward trend, while the disaster situation of crops in the South China area is significantly reduced, especially in Guangdong Province. In addition, except for Heilongjiang Province and the Inner Mongolia Autonomous Region, the direct economic losses across the country show a downward trend. Overall, the typhoon disaster losses in the South China area are relatively significantly reduced, while the typhoon disaster situation in the Northern China, especially the Northeast China and the Inner Mongolia Autonomous Region, has increased (Fig. 2.17).

Priority Areas Addressed:

Integrated

- Enhance activities to develop impact-based forecasts and risk-based warning.

DRR

- Provide reliable statistics of mortality and direct disaster economic loss caused by typhoon-related disasters for monitoring the targets of the Typhoon Committee.
- Evaluate socio-economic benefits of disaster risk reduction for typhoon-related disasters.

Contact Information:

Member: China

Name of contact for this item: Zhu Xuesong

Telephone: +86-021-54896126

Email: zhuxs@typhoon.org.cn

2.8 Tropical Cyclone Operational Skill Training of CMA

2.8.1 Training Workshops on New Techniques of Marine Meteorological Forecasting (2024)

In March and September 2024, two Training Workshops on New Techniques of Marine Meteorological Forecasting were held at the CMA Training Centre (CMATC) in Beijing. These workshops focus on Marine Meteorological Forecasting, which have been widely concerned by forecasters in coastal areas. The 74 trainees were all forecasters from meteorological services over coastal areas or areas seriously affected by typhoon disasters.

The main contents of tropical cyclones training contained Operational Progress of Typhoon Weather Forecast, Mechanism of Typhoon, New Technology and Methods of Typhoon Forecast and Warning, Typhoon Forecast and Warning Service Cases, etc. During the courses, a variety of training methods were used, such as teaching, practice, communication and discussions. The training lasted for three weeks, including one week of online autonomous training. Through the workshops, the trainees' operational capabilities of applying multi-source data were improved, meanwhile, they were provided with a large number of forecasting and service ideas for reference.

2.8.2 The 9th CMA International Training Course on Tropical Cyclone Monitoring and Forecasting (2024)

The 9th CMA International Training Course on Tropical Cyclone Monitoring and Forecasting will be held from November 25 to December 5, 2024, in Guangzhou, China. The course will be co-organized by the Guangdong Meteorological Service and CMATC (WMO Regional Training Centre-Beijing). The Guangdong-Hong Kong-Macao Greater Bay Area (GBA) branch of the World Meteorological Center (WMC) Beijing will continue to be utilized, supporting the development of a meteorological science and technology innovation corridor and a talent hub for the "Greater Bay Area" through practical international meteorological cooperation.

Priority Areas Addressed:

Meteorology

- Enhance and provide typhoon forecast guidance based on NWP including ensembles and weather radar related products, such as QPE/QPF.
- Enhance, in cooperation with TRCG, training activities in accordance with Typhoon Committee forecast competency, knowledge sharing, exchange of latest development and new techniques.

Contact Information:

Member: China

Name of contact for this item: Zhang Xi

Telephone: +86-010-58995753

Email: zhangxi@cma.gov.cn

Annexes

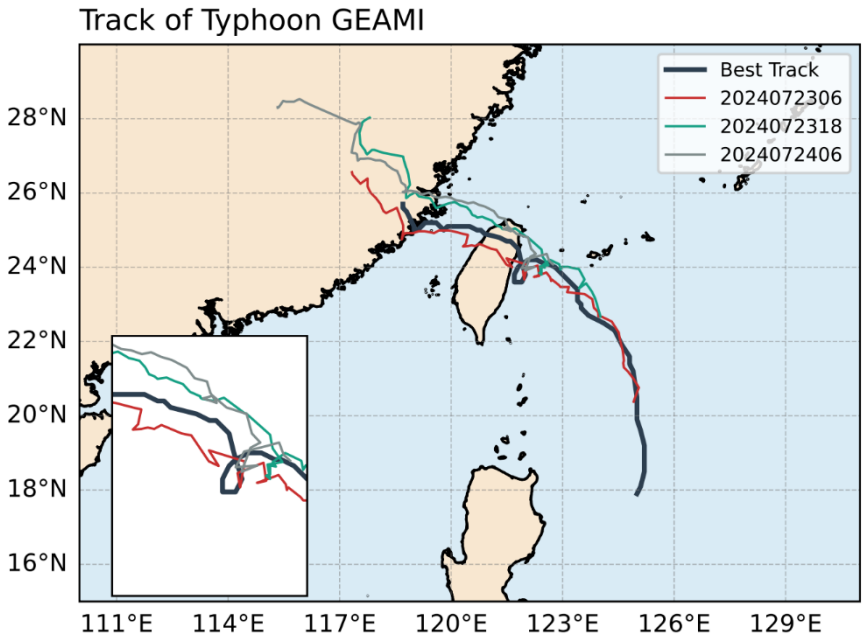

Figure 2.1 The best track of Typhoon Gaemi (2403) in 2024 (dark blue) compared with the forecast tracks from the AITC system at different initialization times (red, green, and gray). The bottom-left inset shows a magnified view of the actual and forecasted looping motion of Typhoon Gaemi east of Taiwan Island.

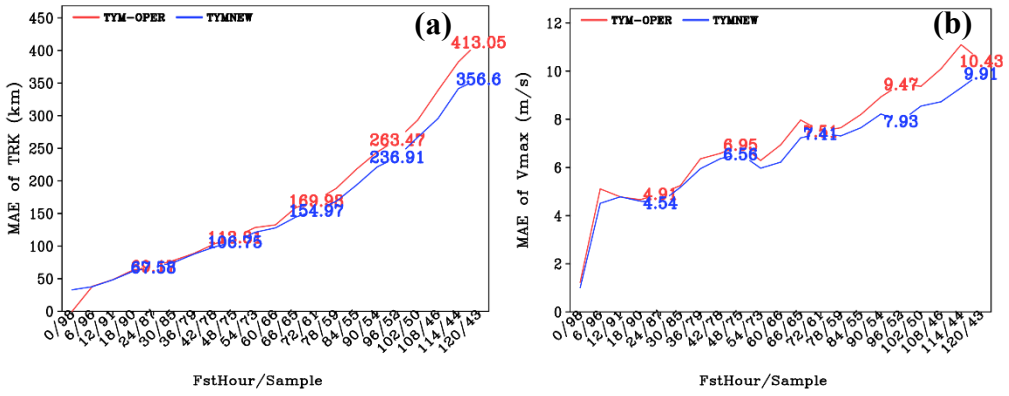

Figure 2.2 Comparisons for (a) TC tracks and (b) TC intensity between the newest (blue lines) and former version (red line) CMA-TYM

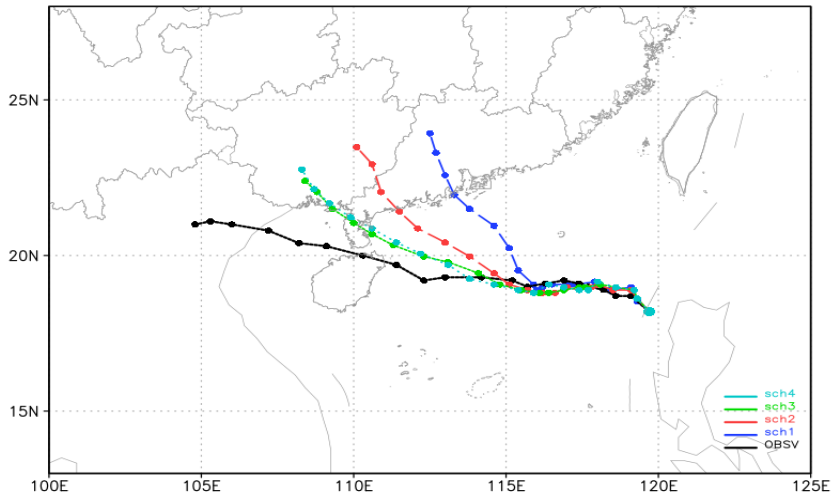

Figure 2.3 Comparison of CMA-TRAMS forecasted tracks of Typhoon Yagi (original scheme sch1, improved schemes sch2, sch3, sch4) with the observed track (black curve).

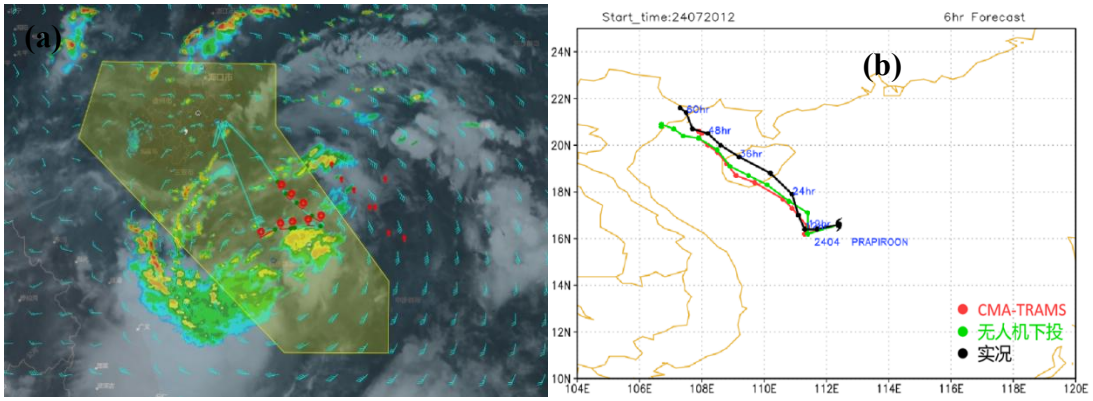

Figure 2.4 (a) Observed air lines of high altitude UAV over the South China Sea; (b) comparison for the forecast track of Prapiroon that assimilated observations of UAV (green line) with the original (red line), the black line represent the real-time TC track of Prapiroon.

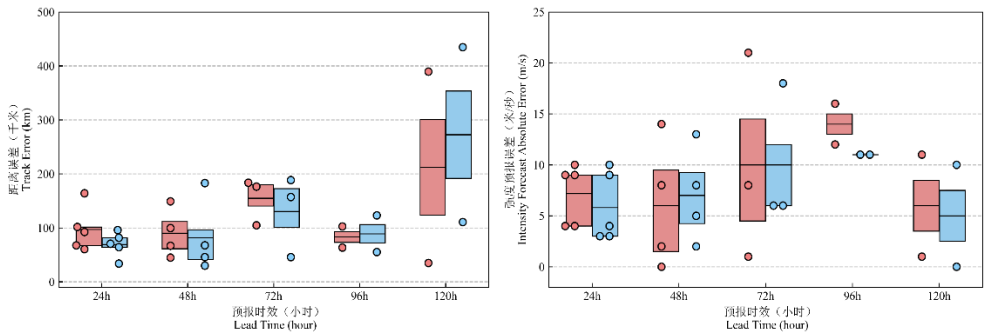

Figure 2.5 Forecast errors of the track (left) and intensity (right) of Typhoon Gaemi before and after the assimilation of external observational data.

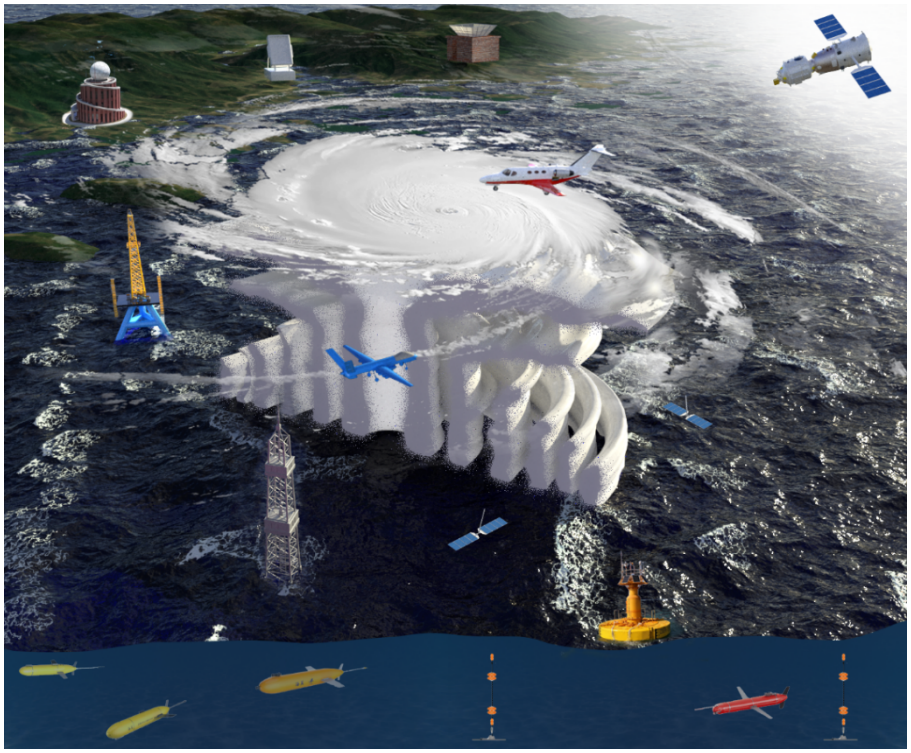

Figure 2.6 Illustration of the comprehensive collaborative observation experiment for TCs in the South China Sea.

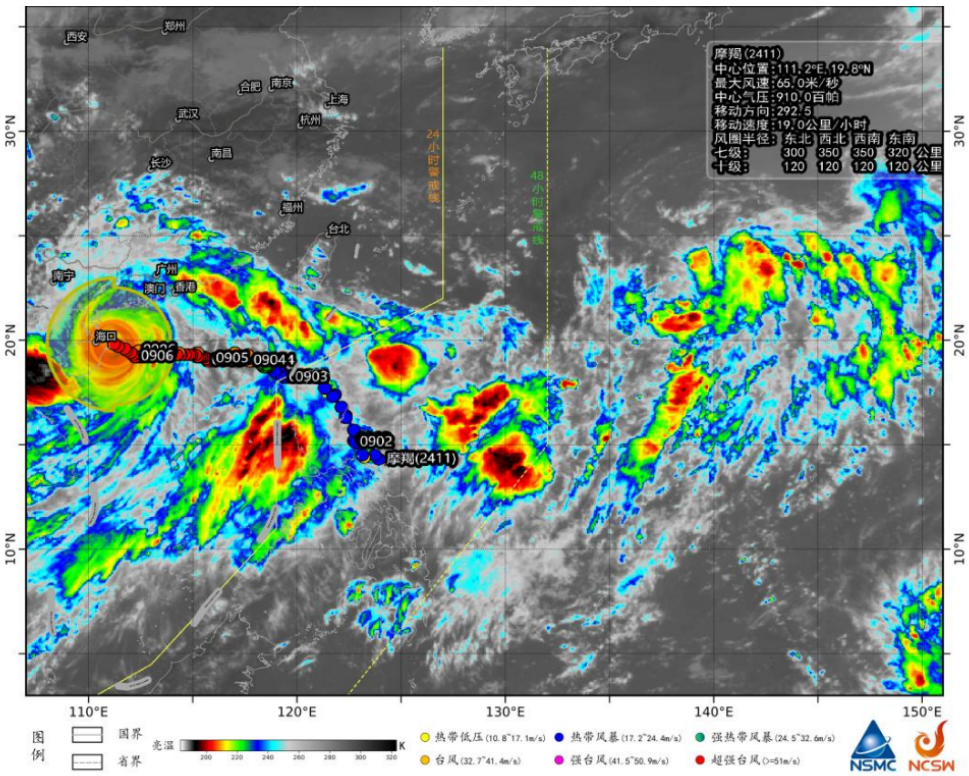

Figure 2.7 Tracks of TCs and the real-time satellite image at 07:00UTC 6th September.

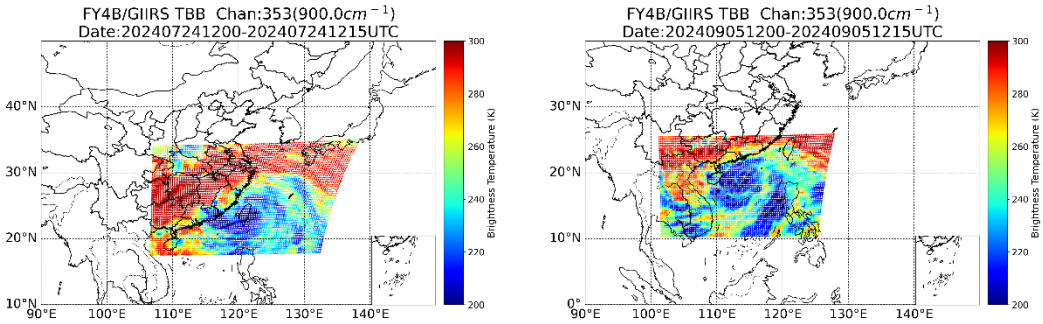

Figure 2.8 Fengyun 4B satellite intensive observation area for Typhoon Gaemi (left, 05:00UTC on 24th July) and typhoon Yagi (right, 00:00UTC on 5th September).

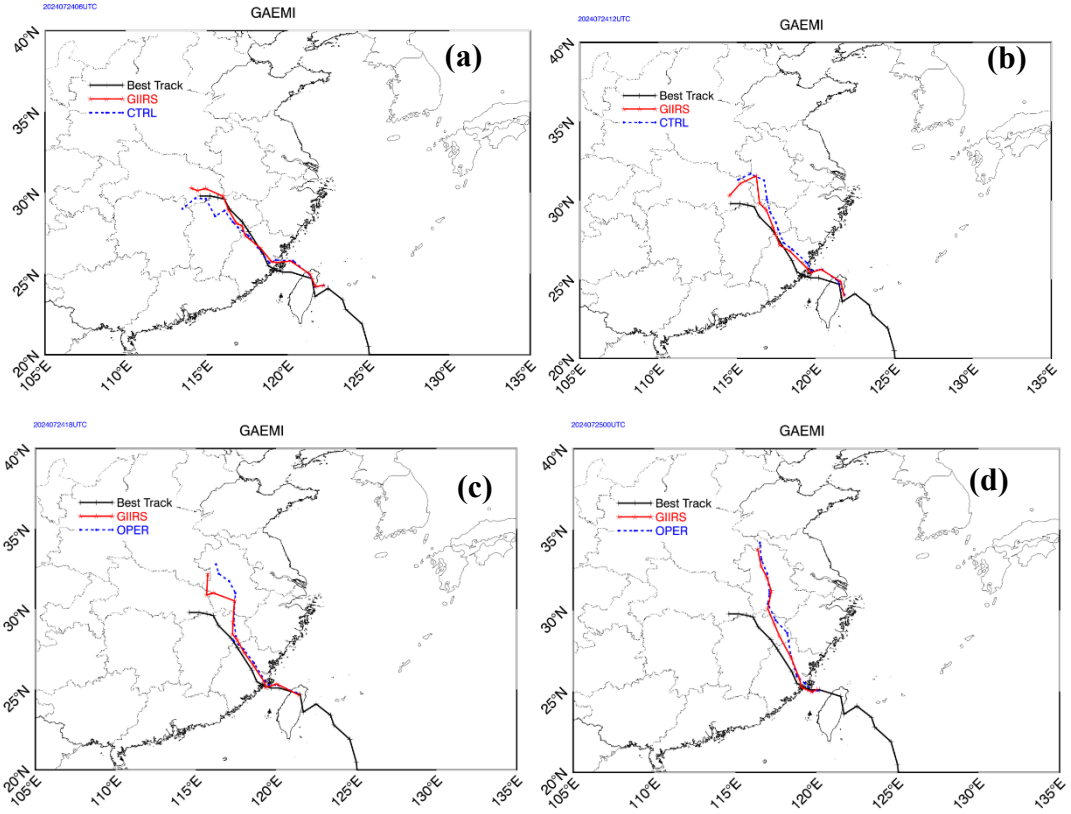

Figure 2.9 The comparisons of Typhoon Gaemi track forecasts with the starting time being 06:00UTC (a), 12:00UTC (b), 18:00UTC (c) on 24th July and 00:00UTC (d) on 25th July, respectively. The black solid line is the real-time observation, the red solid line is the result of assimilating Fengyun 4B GIIRS observations, and the blue dotted line is the control run.

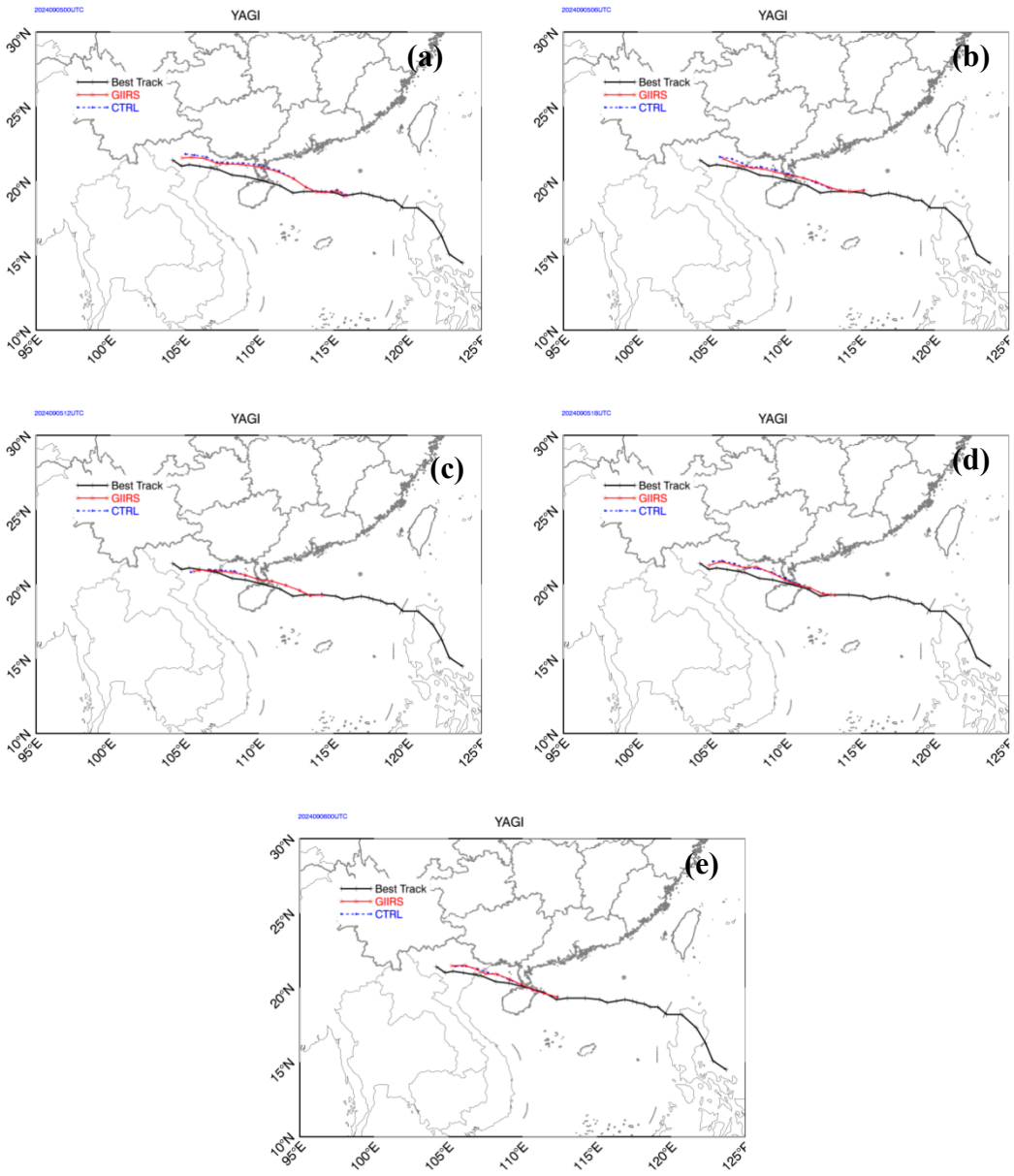

Figure 2.10 The comparisons of Typhoon Yagi track forecasts with the starting time being00:00UTC (a), 06:00UTC (b), 12:00UTC (c), 18:00UTC (d) on 5th September and 06:00UTC (d) on 6th September, respectively. The black solid line is the real-time observation, the red solid line is the result of assimilating Fengyun 4B GIIRS observations, and the blue dotted line is the control run.

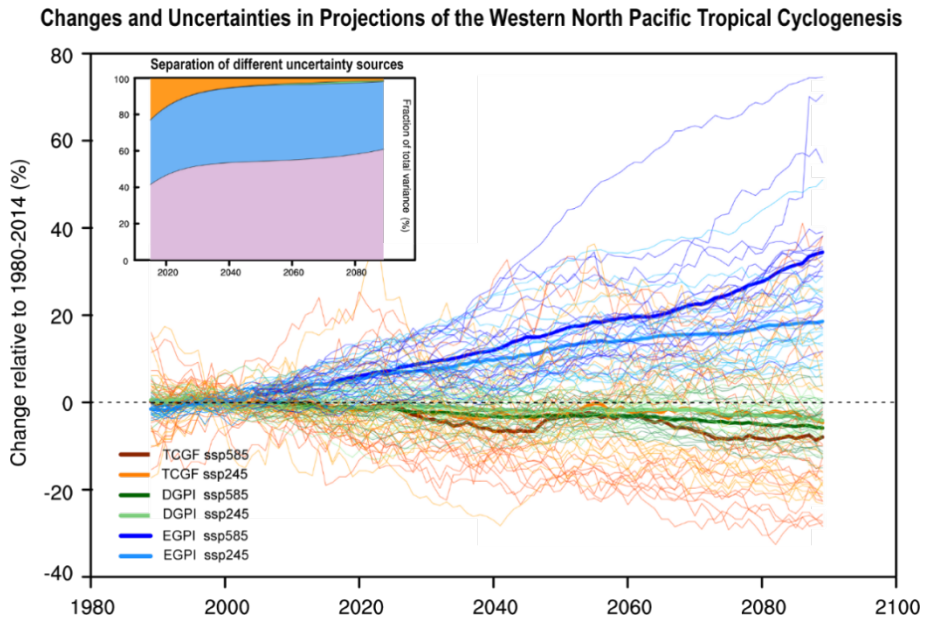

Figure 2.11 Future projections of tropical cyclogenesis in the western North Pacific in CMIP6 climate models. Thin lines denote individual models and thick lines represent the multi-model-mean. Three different schemes are used as a proxy of TC formations, respectively. Projections based on each scheme are analyzed under the moderate-emission (SSP245) and high-emission (SSP585) scenarios. The insert figure on the top left shows the evolution of fractional contributions of different uncertainty sources to total uncertainties. The total uncertainty is separated into four different components, including internal variability (orange), scenario uncertainty (green), model uncertainty (blue) and scheme uncertainty (purple).

Table 2.1 comparison experiment(the best result is represented in bold, followed by underline).

Method	Wind speed MAE	Wind speed RMSE	Wind speed MBE	Wind direction MAE
Bicubic	1.38	1.86	-0.25	99.55
Bilinear	1.38	1.86	-0.25	99.60
IDW	1.37	1.86	-0.29	99.98
Wind-Topo	1.23	1.65	<u>0.23</u>	**78.37**
DeepCams	1.23	1.68	-0.48	97.95
RCM-emulator	<u>1.18</u>	<u>1.64</u>	-0.47	96.17
Uformer	1.24	1.70	-0.77	99.10
TerraWind	**0.79**	**1.24**	**-0.18**	<u>80.62</u>

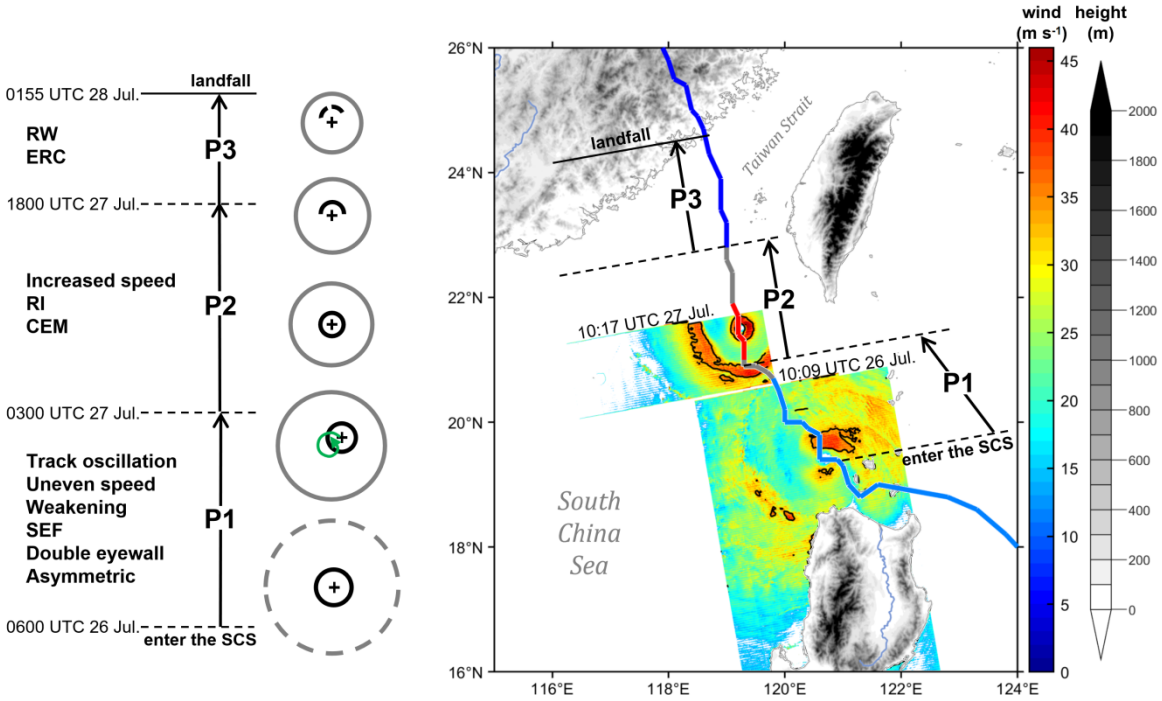

Figure 2.12 Conceptual diagram of Doksuri (2023) over the northeastern part of the SCS, in which the track oscillation, intensity variation, and structural evolution is illustrated. The cross represents the TC center. The gray (black) concentric rings indicate the outer (inner) eyewall. The semicircle indicates the asymmetric and decayed inner eyewall. The color shading illustrates the SAR wind (Unit: m s^{-1}). The red (dark blue) plot indicates the RI (RW) process, the light blue plot indicates the weakening process with a decreasing intensity < 10 m s^{-1} over 12 hours, and the gray plot indicates that the TC intensity is steady.

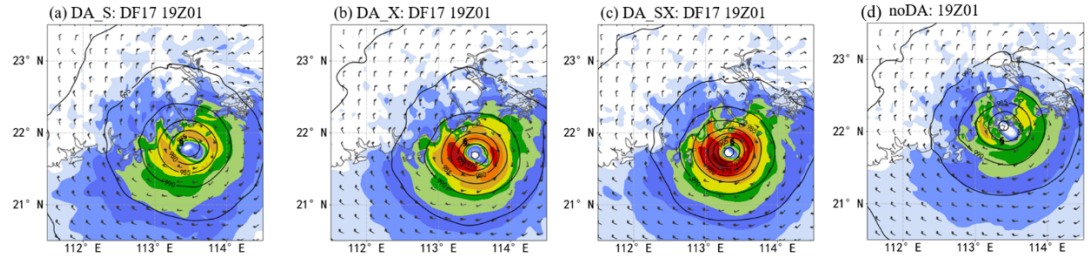

Figure 2.13 Surface level pressure (SLP) (contour, hPa) with 10m horizontal wind speed (shaded, m/s; barbs, each short line represents 2m/s) from (a) DA_S, (b) DA_X, (c) DA_SX and (d) noDA experiment at 1900UTC 1 September 2023. Black dot represents observation position of Saola.

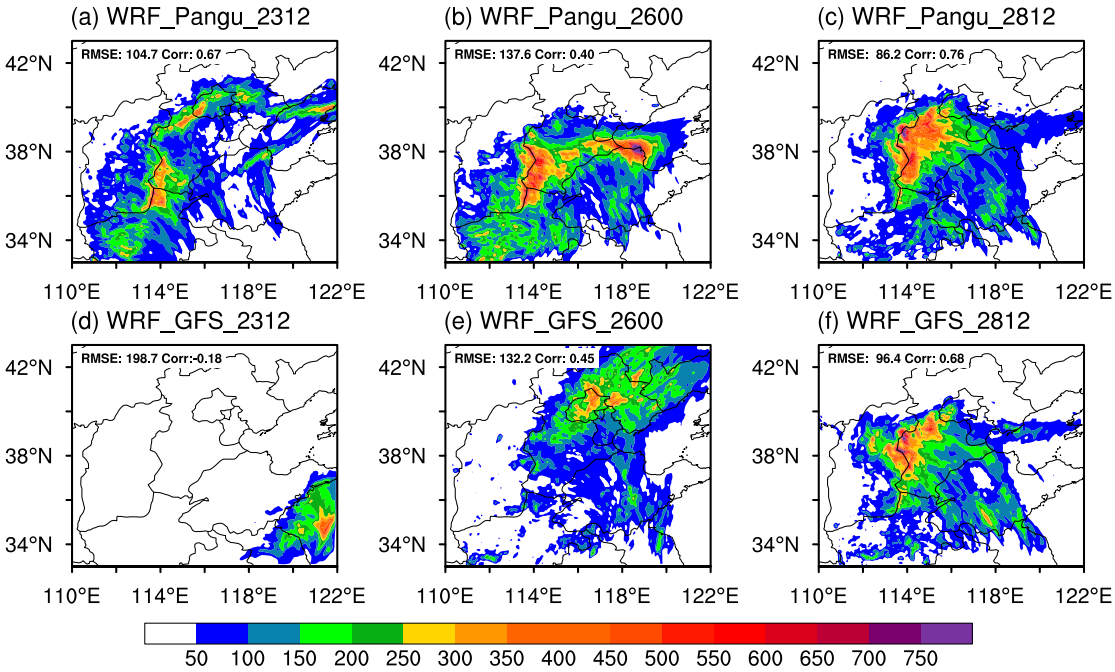

Figure 2.14 The 72h accumulated precipitation (units: mm) between 0000 UTC on 29 July and 0000 UTC on 1st August 2023 for the (a) WRF_Pangu_2312, (b) WRF_Pangu_2600, and (c) WRF_Pangu_2812 simulations. (d-f) are same with (a-c) but for the WRF_GFS simulations.

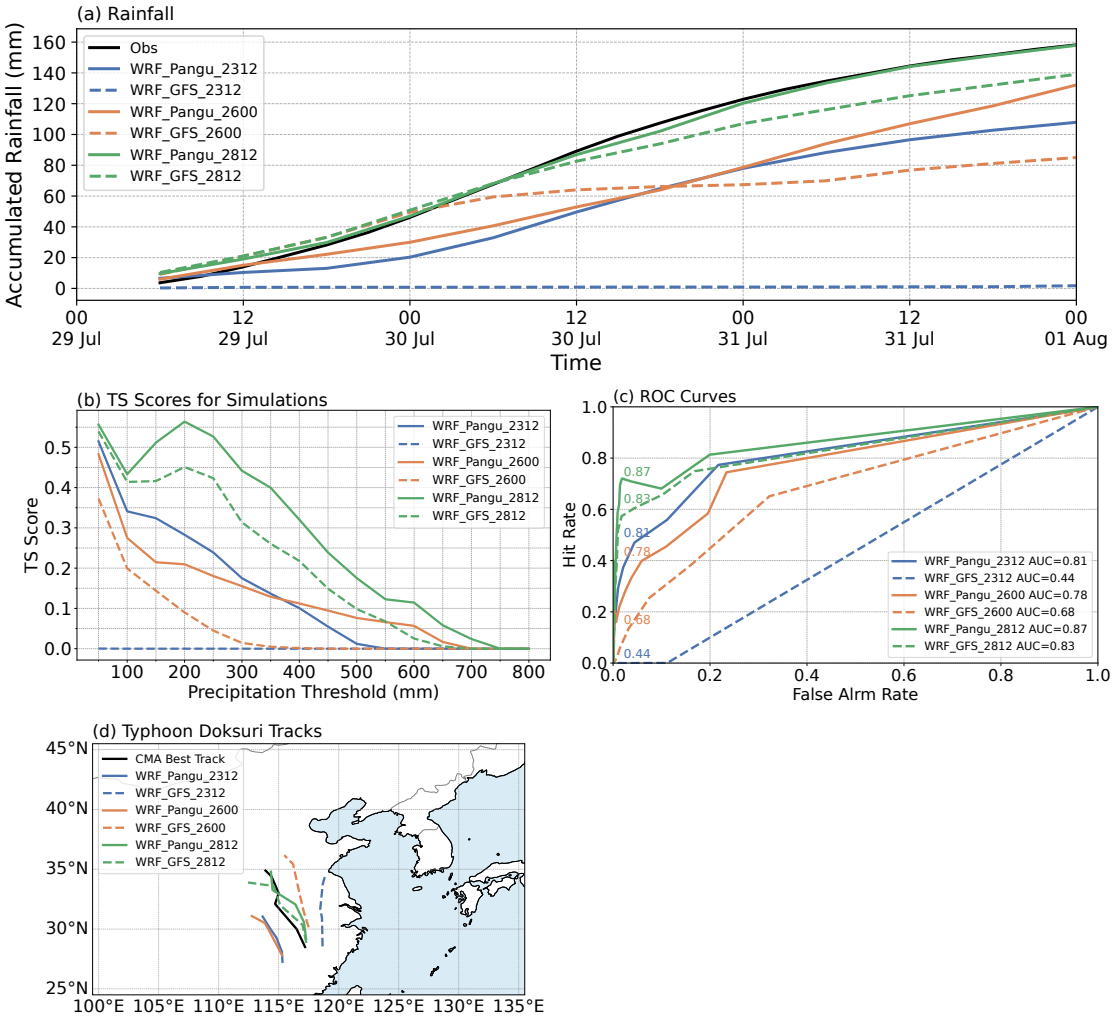

Figure 2.15 (a) Time series of accumulated rainfall (units: mm), over the region demarcated by the red box in Fig. 1a, as derived from both the CMA observational dataset and the WRF experiments. (b) TS, and (c) ROC diagram for the 72-h accumulated rainfall between 0000 UTC on 29 July and 0000 UTC on 1 August 2023 in different experiments against CMA precipitation analysis, and (c) Best-track data from the China Meteorological Administration (CMA, black) and the simulated tracks from the WRF experiments for Typhoon Doksuri, from 0000 UTC on 29 July to 0000 UTC on 30 July 2023.

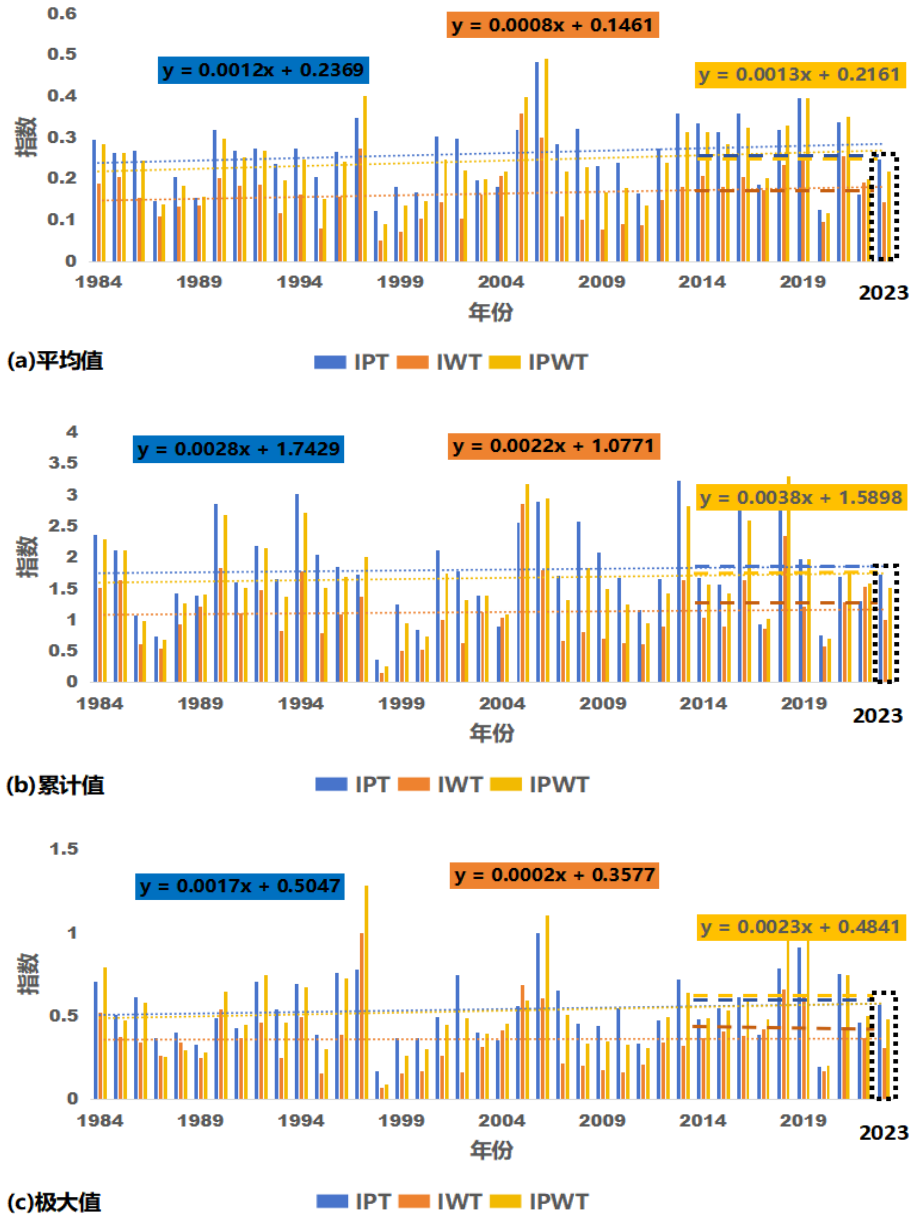

Figure 2.16 The average (a), cumulative (b), and maximum values (c) of the typhoon precipitation impact index, wind impact index, and comprehensive wind-rain impact index from 1984 to 2023. The short, thick dashed lines in corresponding colors represent the average values for the last 10 years (2014-2023).

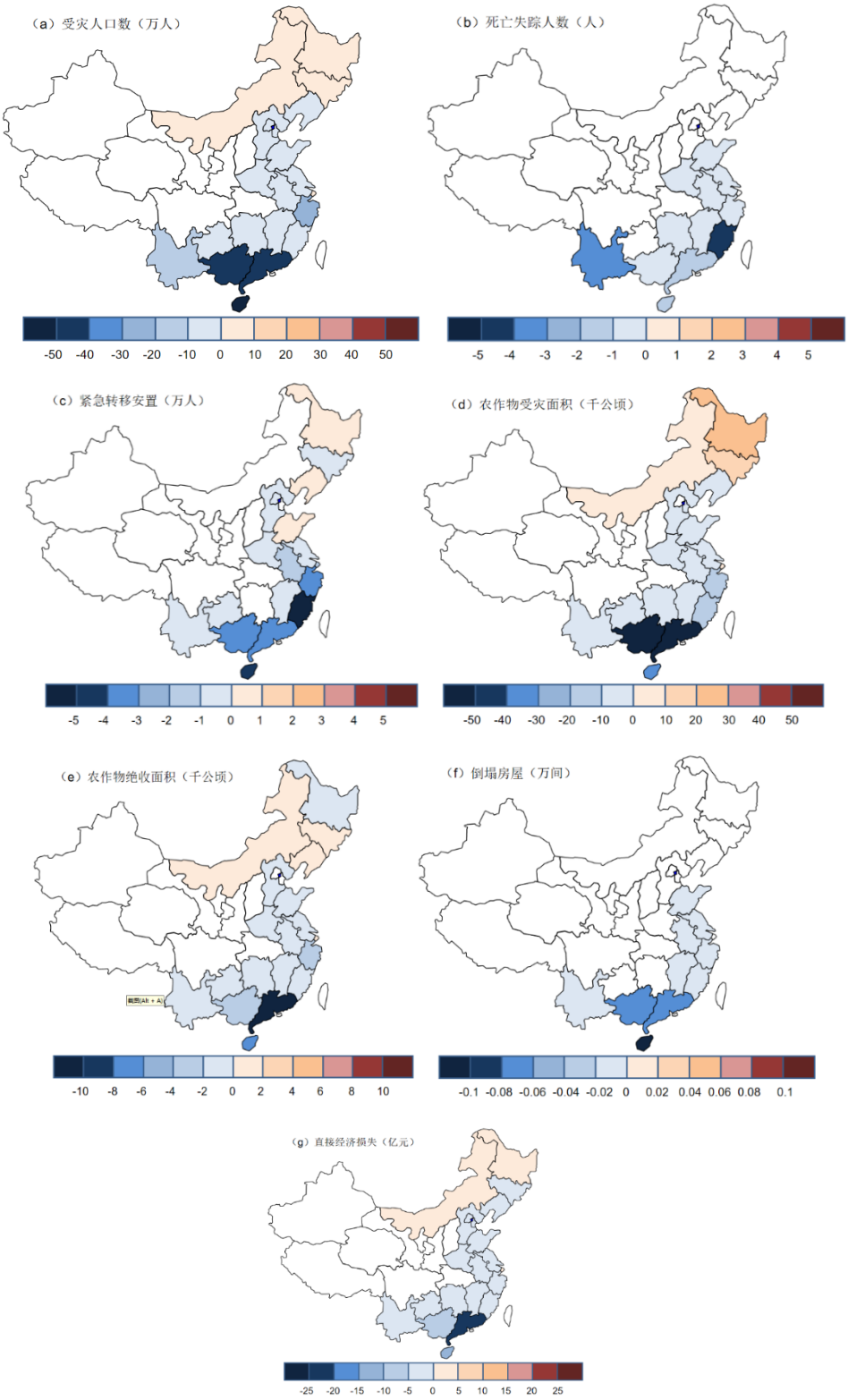

Figure 2.17 The trend of annual totals of typhoon disaster-induced impacts across provinces from 2014 to 2023, including the number of affected people (in ten thousand) (a), the number of people urgently relocated (in ten thousand) (b), the number of deaths and missing persons (people) (c), the area of crop damage (in thousand hectares) (d), the area of complete crop failure (in thousand hectares) (e), the number of collapsed houses (in ten thousand rooms) (f), and the direct economic loss (in billion yuan) (g).